Two-layered structure in the lowermost mantle beneath the southwestern Pacific(Dissertation_全文)

AUTHOR(S):

Yamada, Akira

学位申請論文

山田 朗

主論文

Two-layered structure in the lowermost mantle beneath the southwestern Pacific

Akira Yamada

Department of Geophysics, Kyoto University, Kyoto, Japan

Abstract. The heterogeneities in the D" layer beneath the southwestern Pacific are investigated by using the combination of earthquakes around the Fiji Islands and receivers in the Japanese Islands. The data of short-period P wave are processed by the double-array stacking, a method to stack simultaneously the records from different events. The estimated depth of the D" reflector varies from 270 km to 170 km in the southwestern Pacific. The numerical experiments using various P-velocity models are performed and the rapid velocity increase well explains the waveform of PdP. This increase may be at the top surface of the high-velocity layer (or high-velocity lamella).

The data of broad-band transverse component are also examined. The D" reflection (SdS) is clearly seen in some traces. The polarities of SdS are almost the same as those of the direct S waves, which supports the D" reflector with the rapid S-wave velocity increase with depth, as well as for P wave. While the residuals of differential travel time of ScS-S show fairly large variations, they show systematic large delays of ScS travel times. These delays may be caused by the existence of an S-wave low velocity layer right above the CMB.

A probable cause of both P- and S-waves high-velocity anomaly is considered to be subducted slab material. The low S-velocity layer underlying the high-velocity anomaly might form a shape like a dome, which could be a seed of mantle plume.

Introduction

The lowermost mantle, the D" layer, is one of the most curious region in the earth, because of its strong heterogeneities, its nature as a thermal boundary layer between the liquid iron-alloyed core and the solid silicate mantle and its important role on the earth's dynamics [e.g., review by Loper and Lay, 1995]. Several hypotheses are proposed on the origin of the D" layer: the graveyard of the subducted slab material [e.g., Hofmann and White, 1982], the accumulation of the products caused by the chemical reaction between the lowermost mantle

and outer core [Jeanloz, 1990] and recently, the accumulation of the extraction by the crystallization of the inner core [Ito et al., 1995]. The correlation between the seismological heterogeneity in the deep mantle and the past subduction zones is discussed by Richards and Engebretson [1992]. The heterogeneities in D" by the chemical reaction could be related with the temperature variation in D".

The variations in the wavelength of the heterogeneities have a range from a few thousands kilometers, inferred from the global tomographic technique [e.g., Sengupta and Toksöz, 1976; Inoue et al., 1990; Su et al., 1994], to a few hundreds kilometers [Haddon and Cleary, 1974; Weber and Davis, 1990; Vidale and Benz, 1993; Krüger et al., 1995; Tono and Yomogida, 1996]. The great size of "avalanches" (subducted slab material) [e.g., Tackley et al., 1993] and the rather small size of "inclusions" by the chemical reaction could be associated with the scale variations of the heterogeneous structure in D".

The aims of this study are to investigate the short-scale D" heterogeneities and to infer the physical and chemical images of the D" layer. We present the results of both data analysis and numerical experiment. We analyse the travel times and the waveforms of direct P and S waves, D" reflections (PdP and SdS) and CMB reflections (PcP and ScS). Figure 1 shows the raypaths of these waves. Throughout this study, the differential travel times between each reflection (PdP, SdS, PcP and ScS) and the direct wave (P and S) are used to compensate the anomalies caused by the heterogeneities beneath the receivers and the epicenters, because the raypaths used here are almost identical to each other in the upper mantle and the crust, where lateral heterogeneities may be strong. The anomalies in the differential travel times will be assumed to be caused by the heterogeneities in the lowermost mantle or departures from reference earth model.

The region sampled in this study is located beneath the southwestern Pacific (Figure 2). The global studies regard the D" layer beneath this region as a "slow" region of the seismic velocities. However, the various velocity models for this region are proposed [Kendall and Shearer, 1995; Weber and Körnig, 1992; Shibutani et al., 1993 and Yamada and Nakanishi, 1996a and b]. The low velocity layer with the thickness of 10 km [Mori and Helmberger, 1995] and up to 40 km [Garnero and Helmberger, 1996] is also suggested in this region.

Data Analysis

Data

The observational records used in this study are grouped into the following three types, (1) short-period vertical-component records from three arrays with diameter sizes of a few hundred kilometers, (2) short-period vertical-component records from an array with of ten kilometers and (3) broad-band horizontal-component records by STS1 seismometers. The station locations are indicated in Figure 3.

Three large arrays in Figure 3 are to observe the micro earthquakes under the national project of earthquake prediction, which are operated by Kyoto University (Disaster Prevention Research Institute), the University of Tokyo (Earthquake Research Institute) and Hokkaido University, respectively (hereafter LA1, LA2 and LA3). The small array located in central Japan is operated by the Japan Meteorological Agency (Matsushiro Seismic Array System, MSAS hereafter). The data analysis by using LA1, 2 and 3 is recently presented in Yamada and Nakanishi [1996a and b] and by using MSAS in Yamada et al. [1996]. The results of these data analyses are used in this paper to obtain clearer image of the D" layer. In addition to the above four arrays for the P-wave analyses, the broad-band records (BB in Figure 3) are analysed to study S-wave structure of the D" layer.

We use earthquakes with deep focus (> 300 km) and large magnitude ($m_b > 5.5$) which occurred around the Fiji Islands. The details about the event selection are found in Yamada and Nakanishi [1996a and b]. The event parameters used in this study are summarized in Table 1. Table 2 shows the range of the epicentral distance and the number of records used in this study.

Figure 4 shows the close-up of the bounce region (beneath southwestern Pacific). We project the distribution of these bounce points and the Fresnel ellipses on the earth's surface. The length scale at the depth of the CMB is about half compared with that on the earth's surface.

Analyses

Short-period P wave. The necessity of using the stacking technique for the analyses of the short-period P wave comes from the following reason. The impedance contrast at the D" reflector must be small, which is inferred from the fact that no or few observations of the short-period P reflections from the heterogeneous D" has been done in a single record. To stack records from different events we use a double-array stacking method [Yamada and Nakanishi, 1996a and b] instead of conventional stacking methods by using the slowness as the unknown parameter.

We stack traces by

$$DA(t,d) = \frac{1}{N}\sum_{i=1}^{N} w_i x_i\Big(t + (T_i^P - T_1^P) + (\delta T_i(d) - \delta T_1(d))\Big),$$

where t indicates the travel time, d the distance of the reflector from the CMB, i index number for the event-receiver pairs ($i = 1, N$, the number of N for each region is listed in Table 2), i =1 the pivot pair, w_i amplitude normalization factor, $x_i(t)$ the observed seismogram, T_i^P onset time of P wave of the i-th pair, and $\delta T_i(d)$ theoretical differential travel time between P and PdP of the i-th pair for the reflector at d km from the CMB. In this study, the range of the d-value for the detection of the D" reflection is from 0 km to 400 km with an increment of 10 km. The amplitudes of all traces are normalized by the maximum peak-to-peak amplitude. T_i^P is read from the original seismogram. The correction for the polarity reversal due to source mechanism is included in w_i. More details about the procedure and the accuracy estimation of this method should be referred to Yamada and Nakanishi [1996a and b].

Broad-band S wave. Two horizontal components of broad-band data are rotated to the radial and the transverse components. We find that the signal-to-noise ratios of the radial components are low in the data used here. Moreover radial-polarized SKS is expected to arrive in the time window between the direct S wave and the CMB reflection (ScS) and may contaminate the D" reflection. Therefore we analyse only transverse components in this study.

The one of the aims of this study is the investigation of the short-wavelength (a few hundred kilometers) heterogeneities in D". To stack records from wide region may average the strongly heterogeneous D" and may possibly show 'ghost' images. The array analysis (stacking procedure) is not appropriate for the data from broad-band seismographs used here because of the wide distribution of stations (Figure 3) and bounce points (Figure 4).

In contrast to the short-period P wave, the D" reflection and refraction of the S wave are observed in the single trace from the long-period data [e.g., Gaherty and Lay, 1992 and Kendall and Shearer, 1995]. We examine the low-pass filtered traces with a cut-off frequency of 0.1 Hz, because the increase of the cut-off frequency from this value decreases the signal-to-noise ratios of the data used in this study.

Results

Short-period P wave. The detailed explanations for the results are described in our recent papers [Yamada and Nakanishi, 1996a and b for three large arrays (LA1, 2 and 3) and Yamada et al., 1996 for a small array (MSAS1, 2 and 3)]. Here we present an outline of these results.

The stacked traces obtained from the above equation are converted to the envelopes by using the Hilbert transform. Figure 5 shows the 2-D images of the envelopes for the regions LA1, 2 and 3. The envelope amplitudes are plotted as a function of the differential travel time with respect to the direct P wave and the distance of the D" reflector from the CMB. It is found that the estimated depths of the D" reflectors vary from 270 km (LA1) to 170 km (LA3). The rather small amplitude of the D" reflection from LA2 can be interpreted as the region LA2 is located in the transition from LA1 to LA3.

The small extent of the MSAS array (Figure 3) leads to that the change of the d-value in the above equation from 0 km to 400 km does not make significant changes in waveforms of 41 stacked traces for MSAS1, 2 and 3. Therefore we cannot determine the reflector depth from the 2-D map as is done for LA1, 2 and 3. However several features can be find as follows.

Figure 6 shows the stacked traces for MSAS1. The D" reflection preceding to PcP can be found in the filtered traces with pass-bands of 0-0.5 Hz and 0.3-0.8 Hz. It is worthy to note that the polarity of this PdP is reversed to that of PcP, which is found by taking the correlation coefficient between PdP and PcP. This indicate that the D" reflector beneath MSAS1 has a negative impedance contrast. The diminishing of PdP with the increase of frequency may be indicative of the finite thickness of the D" reflector that causes this anomalous PdP. The depth of the reflector is estimated to be at 50-100 km above the CMB, inferred from the differential travel time of PdP-P.

The signals of PdP are clear in the stacked traces from MSAS2 (not presented here). The region MSAS2 overlaps with the region LA1 (Figure 4), where the D" reflector at 270 km above the CMB is estimated. The travel times of PdP from the region MSAS2 are consistent with the D" structure at 270 km above the CMB.

No clear signal can be found in the stacked traces for the region MSAS3.

Broad-band S wave. We can find 48 signals of ScS and 25 of SdS for following travel time analyses among 80

traces analysed here. Figure 7 shows the examples of the S reflection from the D" reflector (SdS) and ScS. Also shown in Figure 7 are the synthetics calculated by the reflectivity method and by the IASP91 model [Kennett, 1991]. We find clear SdS with large amplitudes, which is not seen in synthetics. Also found are significant time delays of ScS.

The differential travel times of SdS and ScS with respect to the direct S wave are measured by using the cross-correlation. The polarities of SdS show almost the same as that of S, which indicate the positive impedance contrast at the D" reflector. The residuals of ScS-S, $(T_{ScS} - T_S)_{obs.} - (T_{ScS} - T_S)_{cal.}$, are plotted in Figure 8a. The theoretical travel times of ScS and S are calculated by using the IASP91. The residuals show the positive values in the range of 0.05-7.52 sec, which are explained by the S-velocity reduction of a few percents (0-2% or more) in D". The D" thickness is estimated from the differential travel times of SdS-S (Figure 8b), assuming that the S-velocity structure is the same as that of IASP91 in the depth range from the earth's surface to the D" reflector. The estimated depths of the D" reflector range from 70 km to 400 km above the CMB. The estimation of depths of the D" reflectors depends on the S-velocity model. If we increase (decrease) the S velocity by 3% with respect to IASP91 in the lowermost mantle, the estimated depth of the D" reflector deepens (shallows) by about 50 km. We are confronted with the same problem of model dependence when translating the positive ScS-S residuals into the values of the S-velocity reduction in the lowermost mantle. Therefore the quantitative estimations may involve a great uncertainty and we discuss in later section the qualitative features of D"; the positive contrast at the reflector and the S-velocity reduction.

Numerical experiments

The difference in the waveform of the D" reflection, caused by the difference of the structure in D", is examined by using the synthetic seismograms calculated by the reflectivity method. The synthetics for this test are calculated for the event-receiver geometries of the array LA3. The convolution of the instrumental response of the seismographs of this array (short-period vertical component, free-period of 1.0 sec and damping factor of 0.7) is applied to the synthetics. The dominant frequencies of the synthetics range from 0.1 Hz to 1.0 Hz. The double-array stacking is used in the data processing of the synthetics in the same manner as is used to the observed data.

Models of velocity change

The P-velocity models to calculate the synthetics are grouped into five types. They are (1) a lamella with high P velocity, (2) a lamella with low P velocity, (3) a transitional increase in P velocity, (4) a transitional decrease in P velocity and (5) a stack of lamellae. Weber [1994] presents the results of a preliminary analysis of travel time and slowness for the models of high- and low-velocity lamella. For the cases of (1)-(4), three values of 10, 30 and 50 km for the thickness of the lamella or the transition zone are tested. For the stack of lamellae, we use three values of 10, 30 and 50 km as the intervals that separate each lamella of 30 km thick with high P velocity. In all the models the contrast of the P velocity is set to be 3% and the depth of the top surface of the velocity change is located at 2605 km. We have already estimated the impedance contrast and the depth of the reflector in our recent paper [Yamada and Nakanishi, 1996b]. However, the change of either contrast or depth affects the amplitude or the travel time of PdP, respectively, and does not alter the waveform itself. The values of 3% and 2605 km are taken from PWDK model in Weber and Davis [1990] as an example. The P-velocity model of PWDK itself is also used as an example for the D" structure with a discontinuous (abrupt) increase in the P velocity. The IASP91 includes several discontinuities, Moho, upper mantle discontinuities at the depths of 210, 410 and 660 km and has the change in the velocity gradient in the lowermost mantle (2740 km depth). The secondary waves caused by the reflection and the conversion at these discontinuities may contaminate the time window followed by the direct P wave, where PdP is expected to arrive. The synthetic calculation and data analysis by using IASP91 model are made to examine this possibility.

In all the models, the values of both density and quality factor are taken from PREM [Dziewonski and Anderson, 1981]. The S-velocity and density profiles in the lowermost mantle are perturbed in the same manner as the P velocity.

Results of numerical experiments

The results are shown in Figures 9a-i. The characteristics of the D" reflections for the various models are in the following.

PWDK model. PdP signal is well reproduced in third panel of Figure 9a with almost the same waveform

(polarity) as the direct P wave (top). We find that an area circled by the highest contour line for PdP extends in the vertical (depth) range of about 80 km. We also find the deviation of the estimated value of 270 km (indicated by a broken line in second panel) from the exact one of 284 km (2605 km depth from the earth's surface). The flatness of the high PdP energy and the deviation from the correct depth of the D" reflector suggest that the resolution of the determination of the D" reflector depth is a few tens kilometers.

Lamella with high velocity. Among three results from three high-velocity lamella models whose differences are in the thickness of the lamella, Figure 9b shows the result from the lamella with the thickness of 30 km.

The waveform of PdP (third) is distorted with respect to that of the direct P wave (top), due to the interference of reflections from the top surface (normal polarity) and the bottom surface (reversed polarity) of the lamella. The second upward swing in PdP waveform corresponds to bottom-side reflection, which is not seen in PdP from the PWDK model (Figure 9a). Comparing three results obtained from three thicknesses of the lamella, it is found that the increase of the thickness increases the amplitude of PdP. This is because a long wavelength wave is not sensitive to thin lamella. The amplitude of PdP for the 30 km-thick model is comparable to that for the PWDK model. The thickness of 30 km is an approximate wavelength of 2 sec P wave in the lowermost mantle.

Lamella with low velocity. The interference of two reflections from both surfaces of lamella is also found for this model. Figure 9c shows the result for the low-velocity lamella with the thickness of 30 km. In contrast with the previous high-velocity lamella, the wavetrain of PdP consists of the first-arrival reversed reflection (top surface) and secondary-arrival normal reflection (bottom surface). The separation between two reflections is obvious for the lamella with thickness greater than 10 km. Two peaks of PdP are seen in the contour map of Figure 9c.

The reflection from the top surface may be qualitatively small, since the seismic energy that arrives at the boundary with negative P-velocity contrast transmits downward more strongly than that at the boundary with positive P-velocity contrast. Moreover the incident angle of the wave at the bottom surface of the lamella is rather steep in low-velocity lamella and this also leads to the smaller reflection coefficient at the bottom surface. Therefore the amplitudes of these two reflections are smaller than that for high-velocity lamella.

Transitional increase in P velocity. Figure 9d shows the result for the model characterized by a transitional increase in P velocity with the thickness of 30 km. In this case, the amplitude and the waveform of PdP are almost identical to that for the PWDK model. The comparison of three results by changing the thickness from 10 km to 50 km shows that the amplitude of PdP decrease with the increase of the transition zone thickness. The amplitude decreases to a half with the increase of the thickness from 10 km to 50 km. This is because the high-frequency content of the incident wave becomes insensitive to the transition zone as it becomes wide. We also find a continuous trend of delay of the travel time of PdP, correlating with the increase of the thickness. However the time delay of PdP accompanied with the change of the thickness from 10 km to 50 km is small, about 1 sec.

Transitional decrease in P velocity. The result for the model of the transitional decrease in P velocity, with the thickness of 10 km, is shown in Figure 9e. The signal of PdP is characterized by (1) rather small amplitude due to the small reflection coefficient, (2) reversed polarity with respect to that of the direct P wave and (3) rapid diminishing of amplitude with the increase of the thickness of the transition zone. The energy of PdP is beyond the level of a cut-off for plotting the contour map for the model with the thickness greater than 30 km.

Stack of lamellae. The model of the stack of lamellae has a shape like 'teeth'. The contour maps for these show complicated distribution of PdP energy. The reflections at both surfaces of each high-velocity lamella and reverberations inside each lamella and between lamellae form continuous arrivals of seismic energy (PdP-coda).

The differences in the waveform of PdP wavetrain, caused by the change of intervals from 10 km to 50 km, are as follows. **(1) 10 km interval (Figure 9f).** The first arrival is isolated and its shape is almost the same as that for the PWDK model. The PdP-coda is not long in time and not large in amplitude. The thin intervals of 10 km may be ignored by the low-frequency waves. Therefore the thin gap of 10 km is not regarded as a perturbation and the response of this structure to the incident wave is close to the PWDK model. The value of 10 km corresponds to a wavelength of 1.3 Hz. **(2) 30 km interval (Figure 9g).** The wavetrain has a long tail and the first arrival has a large amplitude compared with that of the previous one. In the contour map several peaks follow the first arrival. The complicated system of reflections of this structure makes us difficult to identify origins of these peaks. However the ridge (energy of PdP-coda) extends to the deep region with the

increase of time. **(3) 50 km interval (Figure 9h).** The model consists of four 'teeth' of the high-velocity lamella. Since the intervals are sufficiently wide, signals from each 'tooth' can be separately seen in second and third panels. While the waveform from each 'tooth' is almost identical to that obtained from the model of one high-velocity lamella in Figure 9b, the amplitude is reduced in order of the depth where each lamella is located. The energy from the deepest 'tooth' cannot be found and may be mixed with that of PcP.

IASP91. The result for IASP91 is shown in Figure 9i. The large amplitude of assembly of the direct P wave is shown on the left in contour map. Since the double-array stacking is to enhance the signal from the reflector with common depth, the direct P wave, whose turning depths are different each other, cannot make the peak in the contour map. The right-side energy corresponds to PcP. There is no signal in the time window between P and PcP. This shows that any signals, for example, the reflection and conversion from the upper mantle discontinuities, cannot be enhanced by this method. Therefore we can regard the signals between P and PcP in the observed traces as the reflections from the D" reflectors.

Discussion

Figure 10 shows three pairs of the direct P and PdP waveforms observed from three regions LA1, 2 and 3, where the PdP traces are the same as in Figure 5. The waveforms of PdP are clear for LA1 and 3 but not for the LA2. These waveforms are compared with the synthetics obtained in the above section. The significant feature of the observed PdP waveforms is the upward swing of the second peak, which is seen in synthetics for the high-velocity lamella (Figure 9b), but not for the simple discontinuous model (PWDK, Figure 9a). However, the estimation of the thickness of lamella by using the amplitude of PdP is not determined uniquely, because the amplitude depends on both the thickness of lamella and contrast of P velocity. While the stack of lamellae with intervals larger than 30 km produces the same second swing, the large and long tail of PdP coda, apparent in the synthetic, are not seen in the observations; their wavelets are rather isolated. The models with negative contrast at the reflector, including transitional decrease, cannot explain the PdP waveform.

This waveform with the second swing is the consequence of the interference of the normal and reversed polarized wavelets that correspond to the top- and bottom-surface reflections of the lamella. However, Brühl et al. [1996] suggests the possibility that the one-sided discontinuity like PWDK also produces such an interference

if the reflector has a finite size in horizontal direction. They show in their experiments that the reflection wavelet with reversed polarity appears following the normal polarized reflection due to the existence of the "edge" of finite-size reflector.

The time lag between these two reflections and the shape of the combined waveforms depend on the size of the reflector and on the frequency contents of the incident wave. The time lag of $T/2$ (T the period of incident wave) may lead to the large amplitude of the combined reflections for the finite-size reflector, and this time lag is the definition of the first Fresnel zone. As shown in Figure 4, the major axes of regions LA1 and LA3 have the sizes almost comparable with the size of the Fresnel ellipse for P wave. If there are two reflectors beneath the regions LA1 and LA3 with different depths (270 km and 170 km), the waveforms of the observed PdP can be also explained as the effect of the finite-size reflector, without the lamella structure.

The increase of the seismic velocity at the discontinuity is also suggested by the normal polarities of the SdS waveforms. The second swing, which is an evidence for the lamella but against the one-sided discontinuity (e.g., PWDK-like model), is found in several traces, e.g., the observations on the left side in Figure 7. We have confirmed by using the S synthetics (not presented here) that the lamella produces the second swing for long-period S wave, but that the amplitude of second swing is rather weak. Therefore the fact of small amplitude of the SdS second swing in Figure 7 cannot preclude the lamella structure for S wave.

Either the high-velocity lamella or the discontinuity with finite-size is possible and the combination of the two is also acceptable for both P and S wave. While we cannot resolve this non-uniquness, the positive contrast at the top of the reflector may be inferred from the data analysed here.

One possibility of the high-velocity structure's true character might be the subducted oceanic crust, which is proposed by Weber [1994]. It is not clear whether the subducted slab arrives at the lowermost mantle and whether the shape of it is maintained through the penetration process or it stagnants at 660 km discontinuity and falls into the lowermost mantle as "avalanches" [Lay, 1994 and Loper and Lay, 1995]. It could be a plausible interpretation that the subducted slab material extends horizontally with the convective motion in the lower mantle and forms the high-velocity lamella.

The large residuals of ScS-S (Figure 8a) indicate the low velocity for S wave in the lowermost mantle beneath

the regions LA1 and LA2 (no S-wave data is available beneath the region LA3 in this study). Also beneath the region MSAS1, the existence of low velocity layer is suggested from the P wave in Figure 6. There are evidences for the existence of the low velocity layer in the lowermost mantle beneath the southwestern Pacific [Mori and Helmberger, 1995 and Garnero and Helmberger, 1996]. They also suggest that it might be not a global but a regional feature. The inclusions into the lowermost mantle by the chemical reaction may be of great contents of iron compared with that of mantle [Jeanloz, 1990 and Ito et al., 1995]. The great change of the geotherm at the CMB may lead to the existence of thermal boundary layer with a finite thickness [Loper, 1991 and Gaherty and lay, 1992]. It could be possible that the accumulation of the products by the chemical reaction, whose seismic velocity may be lower than that of ambient mantle due to the iron-rich products, acts a role as the thermal boundary layer and can be seismologically found as a low velocity layer.

The two-layered structure inferred from the above description is schematically illustrated in Figure 11. We indicate in this sketch the values of the P-velocity increase within the high-velocity layer (or lamella), which are inferred from the preliminary estimates of the impedance contrast obtained in Yamada and Nakanishi [1996b]. We assume when inferring the P-velocity increase that both the density and the P velocity increase at the same rate. The stack of the low and the high velocity structure, postulated here, changes its total thickness from 270 km (LA1) to 170 km (LA3). Assuming that the thickness of the high velocity layer is unchanged throughout the region sampled here, the low velocity layer thickens in the region LA1. It is one plausible, not sufficiently confident, speculation that this thickened low velocity layer in LA1 is the plume head, which is now processing the upward motion as a "mantle plume" [Mori and Helmberger, 1995]. Unfortunately we can only search one direction among the region surrounding LA1 at present. The further examination of D" structure in the region neighbored on LA1 will provide us with the more clear evidences of this dome and with its horizontal size.

At the end of this section, we should have a statement about the variations in ScS-S residuals and the depths of the D" S reflector, shown in Figure 8. These large variations are anomalous when taking the extent of the Fresnel ellipse (Figure 4) into account and might be interpreted as the existence of more short-wavelength (perhaps, less than one hundred kilometers) heterogeneities. The SdS amplitude (Figure 7) is also anomalous large, interpretation of which might be attributed to whether the great impedance contrast of several tens

percents at the reflector or the focusing effect by heterogeneities with wavelength shorter than the extent of the Fresnel ellipse. Such an anomalous structure cannot be extracted from the P-wave results presented above. The impedance contrast of P wave at the reflector beneath LA1, 2 and 3 may be up to ten percents, if we assume horizontal reflector. The detection of the clear PdP signals (except for LA2) indicates that the wavelength of heterogeneities may be a few hundred kilometers. This differences of scale length of heterogeneities or the impedance contrast between P and S waves might suggest the anomalous D" layer, where the response to the incidence is different between P and S waves.

Conclusion

The analyses of travel time and waveform are applied to the data of both short-period P wave and long-period S wave. We can suggest the following image for the D" layer beneath the southwestern Pacific sampled here. Comparing the observations with the numerical experiments, the high-velocity lamella is the preferred model rather than the first-order discontinuity to explain the waveform of PdP. However the discontinuity model could still be a possible candidate if we take the finite size of the D" reflector into account. The low-velocity layer, coated with this high-velocity layer, is inferred from the large delay of travel times of ScS. The total thickness of these two layers changes from 270 km to 170 km. This heterogeneous structure might be interpreted as the low-velocity dome (a seed of mantle plume) underlying the high-velocity subducted material.

Acknowledgments. Throughout this work I would like to thank I. Nakanishi for many fruitful suggestions and comments. I also thank K. Oike for his supports. The reflectivity code for synthetic calculations was provided by courtesy of M. Weber.

References

Brühl, M., G. Vermeer, and M. Kiehn, Fresnel zones for broadband data, *Geophysics, 61*, 600-604, 1996.

Dziewonski, A. M., and D. L. Anderson, Preliminary reference earth model, *Phys. Earth Planet. Inter., 25*, 297-356, 1981.

Gaherty, J. B., and T. Lay, Investigation of laterally heterogeneous shear velocity structure in D" beneath Eurasia, *J. Geophys. Res., 97*, 417-435, 1992.

Garnero, E. J., and D. V. Helmberger, Seismic detection of a thin laterally varying boundary layer at the base of the mantle beneath the central-Pacific, *Geophys. Res. Let., 23*, 977-980, 1996.

Haddon, R. A. W., and J. R. Cleary, Evidence for scattering of seismic PKP waves near the core-mantle boundary, *Phys. Earth Planet. Inter., 8*, 211-234, 1974.

Hofmann, A. W., and W. M. White, Mantle plumes from ancient oceanic crust, *Earth Planet Sci. Lett., 57*, 421-436, 1982.

Inoue, H., Y. Fukao, K. Tanabe, and Y. Ogata, Whole mantle P-wave travel time tomography, *Phys. Earth Planet. Inter. 59*, 294-328, 1990.

Ito, E., K. Morooka, O. Ujike, and T. Katsura, Reactions between molten iron and silicate melts at high pressure: Implications for the chemical evolution of earth's core, *J. Geophys. Res., 100*, 5901-5910, 1995.

Jeanloz, R., The nature of the Earth's core, *Annu. Rev. Earth Planet. Sci., 18*, 357-386, 1990.

Kendall, J.-M., and P. M. Shearer, On the structure of the lowermost mantle beneath the south west Pacific, southeast Asia and Australasia, *Phys. Earth Planet. Inter., 92*, 85-98, 1995.

Kennett, B. L. N., ed., IASPEI 1991 Seismological Tables, *Publ. Australian Nat. Univ.*, 1991.

Krüger, F., M. Weber, F. Scherbaum, and J. Schlittenhardt, Evidence for normal and inhomogeneous lowermost mantle and core-mantle boundary structure under the Arctic and northern Canada, *Geophys. J. Int., 122*, 637-657, 1995.

Lay, T., The fate of descending slabs, *Annu. Rev. Earth Planet. Sci., 22*, 33-61, 1994.

Loper, D. E., Mantle plumes, *Tectonophysics, 187*, 373-384, 1991.

Loper, D. E., and T. Lay, The core-mantle boundary region, *J. Geophys. Res., 100*, 6397-6420, 1995.

Mori, J., and D. V. Helmberger, Localized boundary layer below the mid-Pacific velocity anomaly identified from a PcP precursor, *J. Geophys. Res., 100*, 20359-20365, 1995.

Richards, M. A., and D. C. Engebretson, Large-scale mantle convection and the history of subduction, *Nature, 355*, 437-440, 1992.

Sengupta, M. K., and M. N. Toksöz, Three dimentional model of seismic velocity variation in the earth's mantle, *Geophys. Res. Lett., 3*, 84-86, 1976.

Shibutani, T., A. Tanaka, M. Kato, and K. Hirahara, A study of P-wave velocity discontinuity in D" layer with J-array Records: Preliminary results, *J. Geomag. Geoelectr., 45*, 1275-1285, 1993.

Su, W.-J., R. L. Woodward, and A. M. Dziewonski, Degree 12 model of shear velocity heterogeneity in the mantle, *J. Geophys. Res., 99*, 6945-6980, 1994.

Tackley, P. J., D. J. Stevenson, G. Glatzmaier, and G. Schubert, Effects of an endothermic phase transition at 670 km depth on spherical mantle convection, *Nature, 361*, 699-704, 1993.

Tono, Y., and K. Yomogida, Origin of short-period P-diffracted waves: A case study of the 1994 Bolivian deep earthquake, *submitted to Phys. Earth Planet. Inter.*, 1996.

Vidale, J. E., and H. M. Benz, Seismological mapping of fine structure near the base of the earth's mantle, *Nature, 361*, 529-532, 1993.

Weber, M., and J. P. Davis, Evidence of a laterally variable lower mantle structure from P- and S-waves, *Geophys. J. Int., 102*, 231-255, 1990.

Weber, M., and M. Körnig, A search for anomalies in the lowermost mantle using seismic bulletins, *Phys. Earth Planet. Inter., 73*, 1-28, 1992.

Weber, M., Lamellae in D"? An alternative model for lower mantle anomalies, *Geophys. Res. Lett., 21*, 2531-2534, 1994.

Yamada, A., and I. Nakanishi, Detection of P-wave reflector in D" beneath the south-western Pacific using double-array stacking, *Geophys. Res. Lett., 23*, 1553-1556, 1996a.

Yamada, A., and I. Nakanishi, Short-wavelength variation of P-wave reflector in D" beneath the south western Pacific, *in preparation*, 1996b.

Yamada, A., A. Kobayashi, and G. Aoki, Detection of the D"-reflector by using a small aperture array, *Technical Reports of Matsushiro Seismological Observatory, JMA, 13, in Japanese*, 1-8, 1996.

Figure captions

Figure 1. Raypaths of waves used here. A square shows the hypocenter at the depth of 500 km and the receiver is indicated by a circle; the epicentral distance is 70° in this example.

Figure 2. The geographical distribution of events (circles) and receivers (squares) utilized here. Also shown are great circle paths connecting event to receiver. The sampling region is beneath the southwestern Pacific (rectangular region). The close-up of this region can be found in Figure 4.

Figure 3. Receiver distribution in Japan. Large arrays with its extents of several hundred kilometers are indicated by blue symbols; Kyoto University (LA1, circles), the University of Tokyo (LA2, triangles) and Hokkaido University (LA3, squares). A green circle shows the location of a small array operated by Japan Meteorological Agency (Matsushiro Seismic Array System, MSAS). The panel on top left shows the close-up of the MSAS. Red circles indicate the distribution of the receivers of the broad-band seismographs (BB).

Figure 4. The bounce point region sampled here (rectangular region in Figure 2). Colored ellipses show the distribution of PcP bounce points, corresponding to arrays in Figure 3. They are LA1 (green), LA2 (blue), LA3 (gray), MSAS1 (yellow), MSAS2 (orange) and MSAS3 (purple), respectively. Solid circles indicate ScS bounce points from broad-band records (BB). Two open ellipses on the bottom left show the first Fresnel ellipses for P wave (0.5 Hz) and S wave (0.1 Hz) at the CMB. Here we plot a half size of the first Fresnel Zone according to Weber and Davis [1990].

Figure 5. The 2-D colored presentation of results by the double-array stacking (the same figure as Figure 3 in Yamada and Nakanishi [1996b]). a) result for region LA1, b) LA2 and c) LA3. In each panel, a signal, that is interpreted as a candidate of PdP, is indicated by an arrow. A trace on each map shows a stacked trace, whose envelope is a cross-section of each map at the depth of the maximum amplitude of PdP. PdP is indicated by a dot in each trace.

Figure 6. The stacked traces from region MSAS1, with the application of several band-pass filters (pass-band is indicated on top right in each trace). Solid circles show the anomalous PdP, whose polarities are opposite to those of PcP.

Figure 7. An example of traces of transverse component from the broad-band seismographs. All traces are

low-pass filtered with the cut-off frequency of 0.1 Hz. The continuous line is the observation and the broken line the synthetics calculated by using IASP91. The epicentral distance is shown in bottom left in each trace.

Figure 8. a) Variation in the residuals of ScS-S. The size of circle is proportional to the amount of the residual. Colored ellipses show the bounce regions of P waves as the same in Figure 4. b) Variation in the thickness of D", that is obtained from the differential travel time of SdS-S. Here we assume that the depth of the D" reflector is the depth of the top surface of the D" layer. The size of circle is proportional to the thickness of the D" layer. P-wave bounce points are also shown.

Figure 9. In all figures from a) to i), (top panel) the stacked synthetic trace of the direct P wave, (second) 2-D contour map with the contour intervals of 1 dB and a signal of PdP is indicated, (third) the stacked trace of PdP, whose envelope is the cross-section at the depth indicated by broken line in second panel and (bottom) the P-velocity structure used to the calculation of the synthetics.

a) result of PWDK, b) high-velocity lamella with the thickness of 30 km, c) low-velocity lamella with the thickness of 30 km, d) transition with increase in P velocity by 30 km, e) transition with decrease in P velocity by 10 km, f) stack of lamellae with intervals, that separate each lamella, of 10 km, g) stack of lamellae with intervals of 30 km and h) stack of lamellae with intervals of 50 km. i) result for IASP91. Because of the lack of any signal between P and PcP, no stacked trace (corresponding to the third panel in figures a-h) is presented.

Figure 10. Comparison of the waveforms between the direct P wave and PdP. a) stacked traces of both waves from region LA1, b) LA2 and c) LA3. The signals of PdP are indicated by horizontal continuous bars, except for LA2 (broken bar), which shows low signal-to-noise ratio compared to PdPs for LA1 and LA3.

Figure 11. Schematic sketch of the D" layer which is obtained in this study. The total thickness of D" varies from 270 km (LA1) to 170 km (LA3). At the top of D", the rapid increase of P and S velocities is inferred. The contrasts of the P velocity across these reflector are also indicated, which are inferred from the preliminary estimations in Yamada and Nakanishi [1996b]. Inferred from the comparison of observed and synthetic seismograms, the high-velocity lamella could be one interpretation for this high-velocity layer. Beneath this layer, there may be a low S-velocity layer, while this is indicated beneath LA1 and LA2 and is unknown beneath LA3.

Table captions

Table 1. Event parameters used in this study. The notations of the column "Data Set" are the same as in Figure 3. Note that MSAS is divided into three regions (MSAS1, 2 and 3) according to the locations of bounce points.

Table 2. The range of epicentral distance and the number of traces for each data set used here. The notations of data set are the same as in Figure 3 and Table 1.

Table 1.

Origin time(GMT)						Lat.	Lon.	Depth	m_b	Data Set
Y	M	D	H	M	S	(°)	(°)	(km)		
1984	Mar.	14	11	36	30.9	20.08S	178.07W	570	5.7	LA3,MSAS2
1984	Jul.	03	13	42	00.83	17.735S	178.847W	536	5.7	MSAS1
1984	Aug.	26	5	00	45.6	23.59S	179.07E	560	5.9	LA3
1984	Sep.	28	3	3	46.8	21.51S	177.79W	364	5.8	LA3,MSAS2
1985	Mar.	15	00	16	02.75	20.682S	178.218W	545	5.7	MSAS2
1985	Aug.	28	20	50	48.3	21.01S	178.98W	625	6.1	LA3,MSAS2
1986	Apr.	01	10	13	40.74	18.037S	178.537W	540	5.8	MSAS1
1987	Feb.	10	00	59	28.57	19.489S	177.456W	395	6.2	MSAS2
1987	Feb.	14	13	38	22.77	17.926S	178.632W	566	5.7	MSAS1
1987	Apr.	29	14	27	35.7	19.01S	177.73W	385	5.9	LA3
1987	Aug.	26	6	56	46.2	20.74S	178.46W	569	5.7	LA3
1988	Jan.	24	16	00	04.55	17.763S	178.737W	566	5.7	MSAS1
1988	Nov.	16	05	53	20.29	21.768S	179.426W	582	5.8	MSAS2
1989	Apr.	18	12	33	52.16	23.834S	179.944E	524	5.8	MSAS3
1989	May	21	21	56	48.63	17.952S	178.593W	584	5.7	MSAS1
1989	Nov.	29	05	48	59.84	25.374S	179.629E	487	5.7	MSAS3
1990	May	17	15	59	56.53	25.398S	178.101E	614	5.8	MSAS3
1990	May	28	11	28	47.69	20.874S	177.987W	486	5.9	MSAS2
1990	Jun.	26	12	08	29.39	22.015S	179.473W	587	6.0	MSAS2
1990	Jun.	29	03	53	28.76	21.552S	179.332W	616	5.7	MSAS2
1990	Aug.	10	17	47	36.78	19.805S	177.385W	373	6.0	MSAS2
1990	Oct.	10	05	54	53.54	23.497S	179.029E	549	6.0	MSAS3
1991	Apr.	18	9	41	20.1	22.92S	179.34W	471	5.7	LA2
1991	Aug.	28	21	32	35.4	22.23S	179.64E	599	5.5	LA1
1991	Sep.	30	0	21	46.4	20.878S	178.59W	566	6.3	BB
1992	Jan.	13	9	37	43.7	20.93S	178.72W	575	5.7	LA1
1992	Apr.	4	1	11	12.3	17.95S	178.37W	574	5.6	LA1
1992	Aug.	30	20	9	5.8	17.92S	178.71W	565	5.8	LA1,2,BB
1992	Nov.	12	22	28	57.5	22.401S	178.10W	360	5.9	BB
1993	Mar.	21	5	4	59.2	18.04S	178.53W	589	6.1	LA1,MSAS1,BB
1993	Apr.	16	14	8	38.9	17.778S	178.86W	565	6.0	BB
1993	Apr.	20	16	26	19.5	20.88S	178.70W	592	5.6	LA1,2
1993	Jul.	9	15	37	53.7	19.78S	177.49W	398	6.0	LA1
1993	Aug.	7	17	53	24.2	23.866S	179.85E	523	6.0	BB
1993	Oct.	11	13	7	29.6	17.85S	178.73W	555	5.8	LA2,MSAS1,BB
1994	Mar.	9	23	28	6.7	18.039S	178.41W	563	6.6	BB
1994	Mar.	31	22	40	52.15	22.057S	179.533W	580	6.1	MSAS2,BB
1994	Oct.	27	22	20	28.5	25.778S	179.34E	519	5.9	BB
1995	Jan.	17	16	54	12.0	20.870S	179.24W	637	6.0	BB

Table 2.

Data Set	Δ (°)	No. of traces
LA1	67.8-71.6	57
LA2	66.0-70.1	31
LA3	70.6-74.4	37
MSAS1	67.4-68.0	48
MSAS2	69.6-70.8	71
MSAS3	71.0-72.9	27
BB	58.4-74.9	80

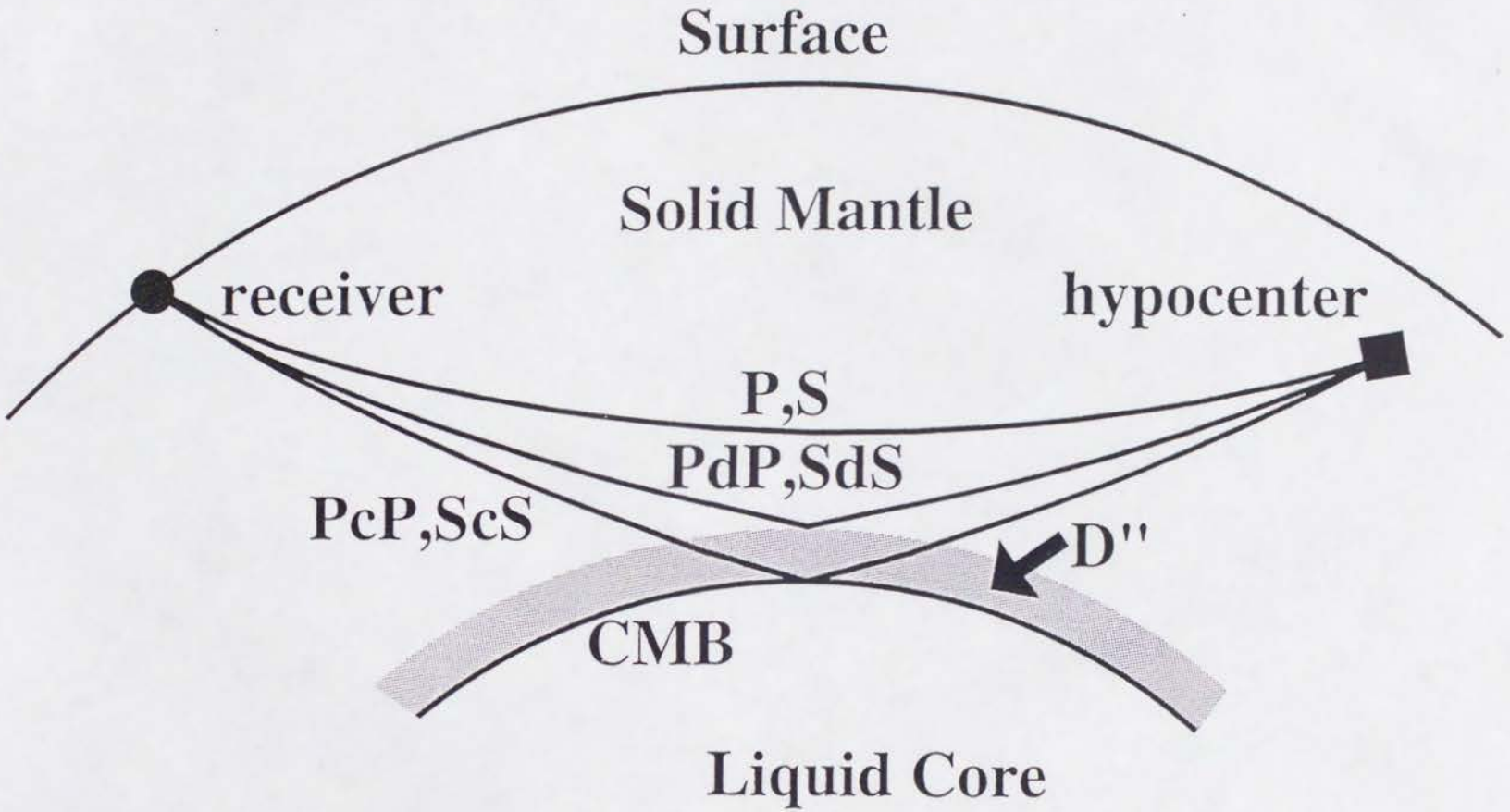
Surface
Solid Mantle
receiver
hypocenter
P,S
PdP,SdS
PcP,ScS
D''
CMB
Liquid Core

Figure 1

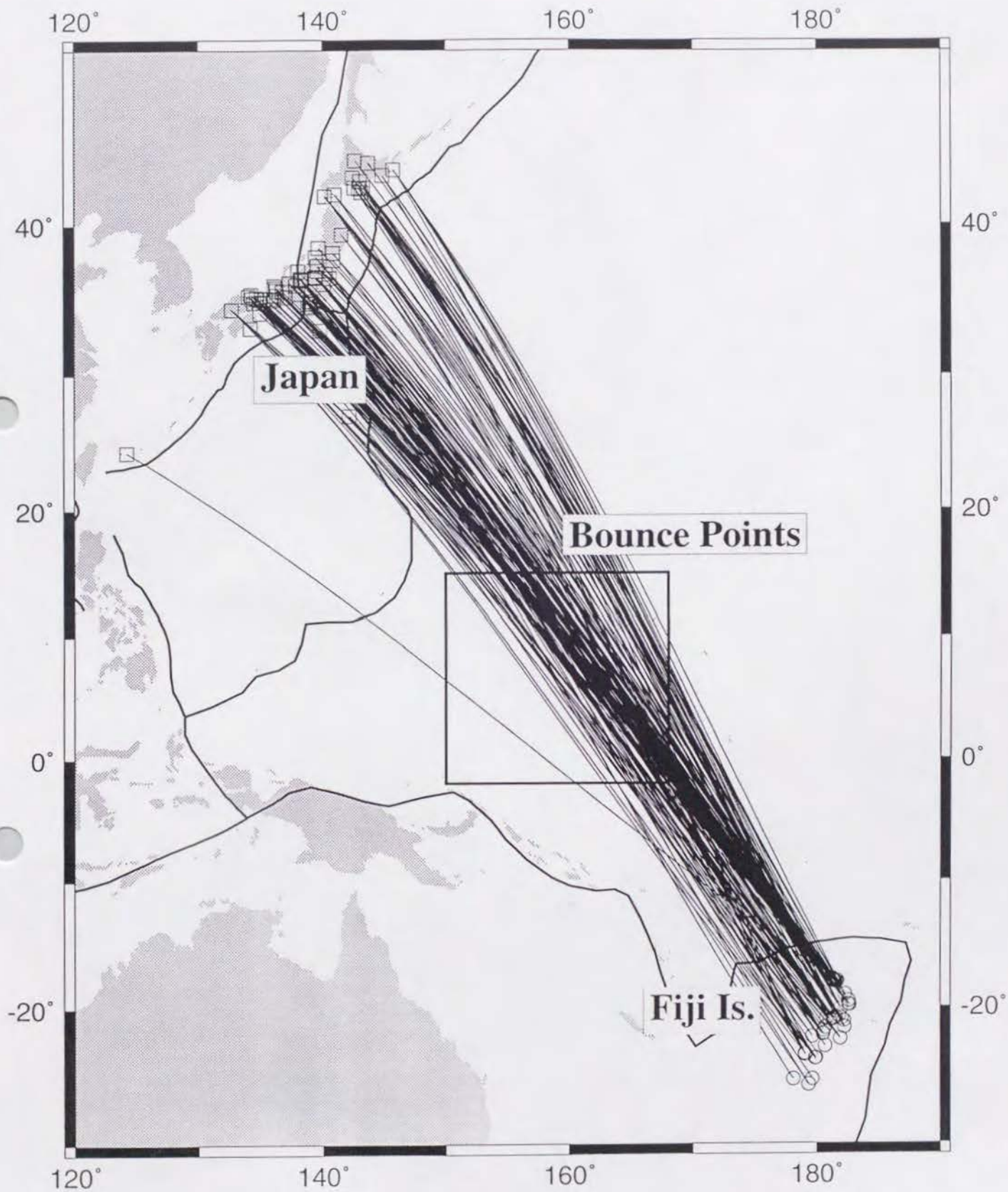

Figure 2

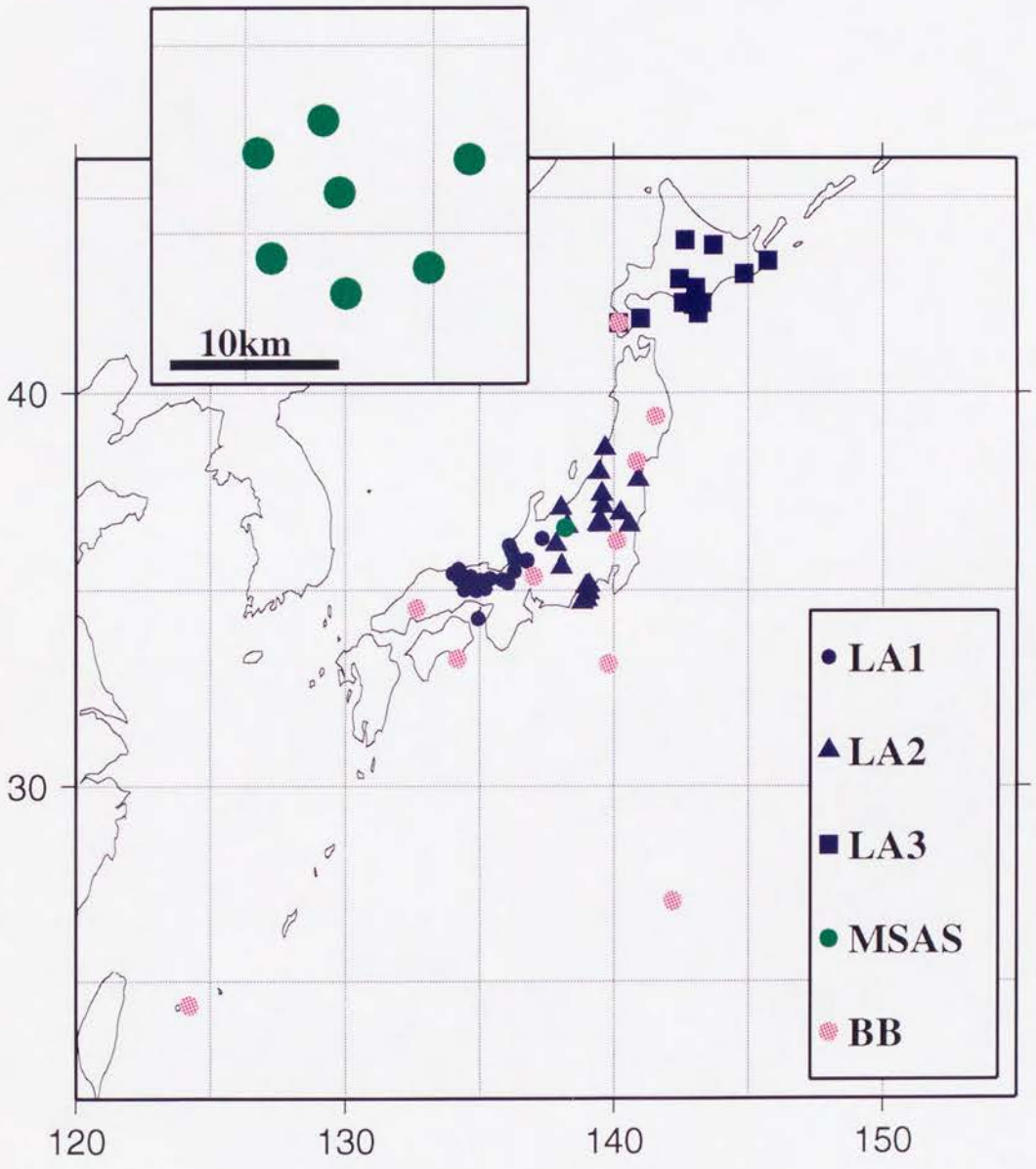

Figure 3

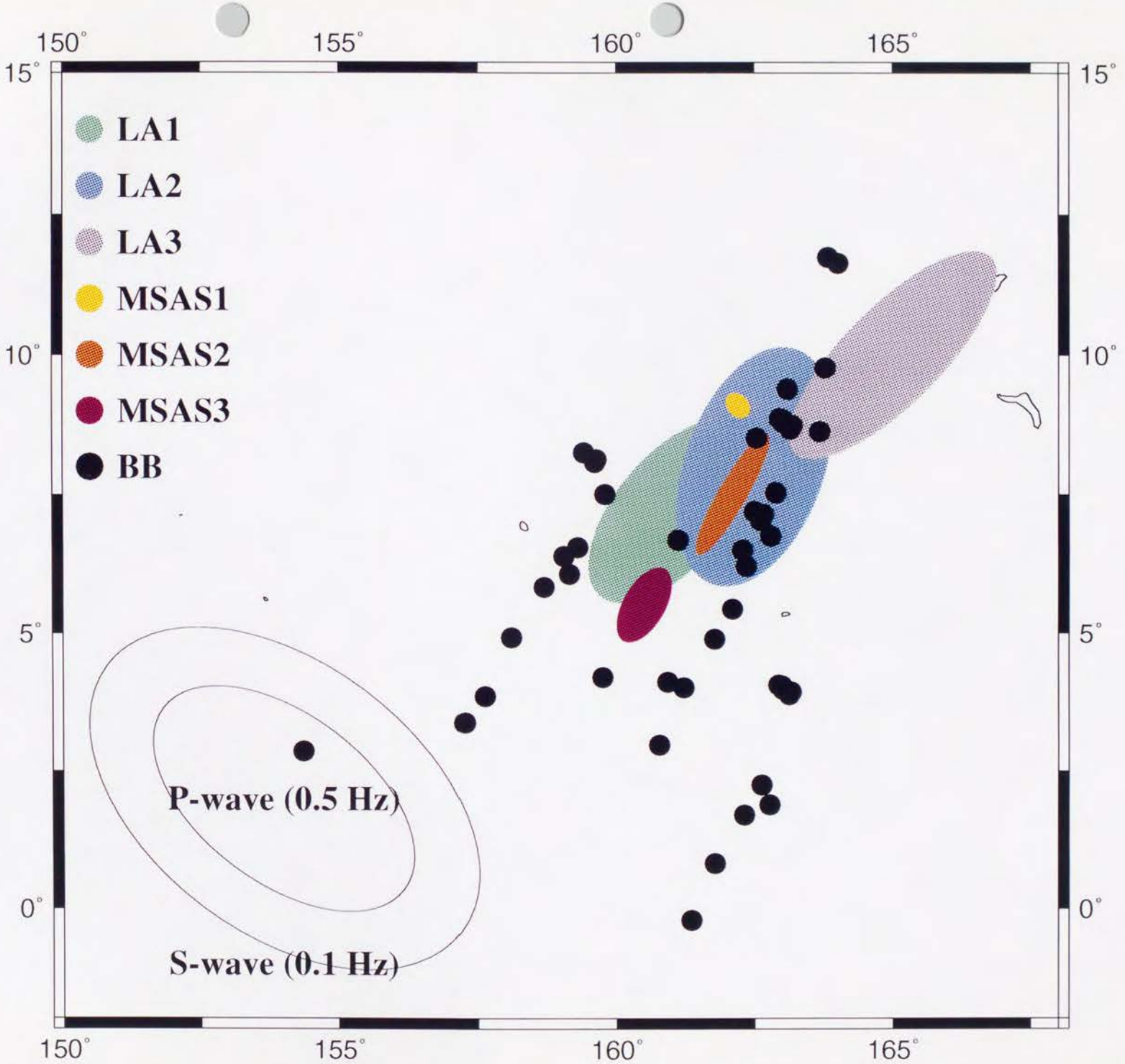
150°
155°
160°
165°
15°
10°
5°
0°
LA1
LA2
LA3
MSAS1
MSAS2
MSAS3
BB
P-wave (0.5 Hz)
S-wave (0.1 Hz)

Figure 4

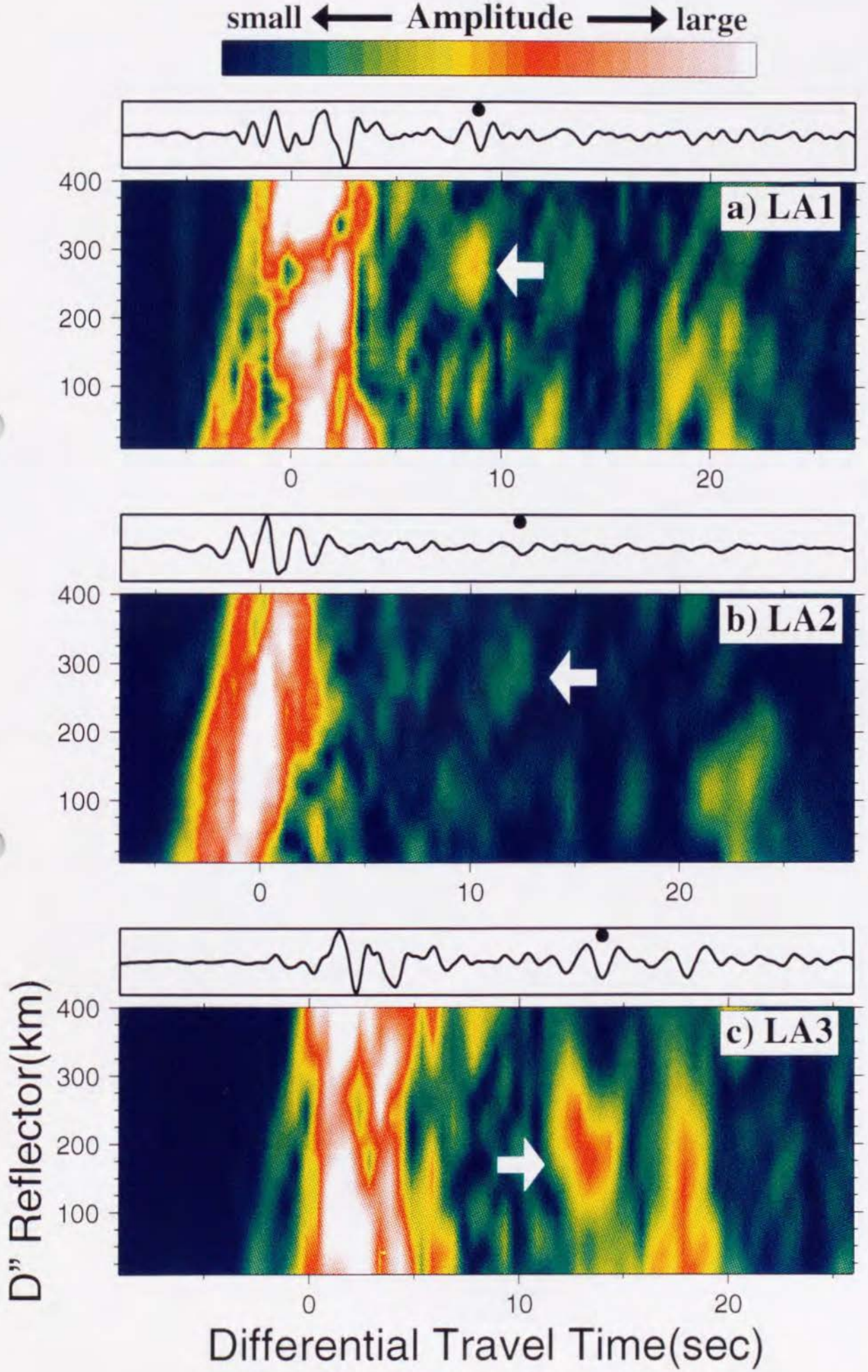
small ← Amplitude → large
a) LA1
b) LA2
c) LA3
400
300
200
100
0
10
20
D" Reflector(km)
Differential Travel Time(sec)

Figure 5

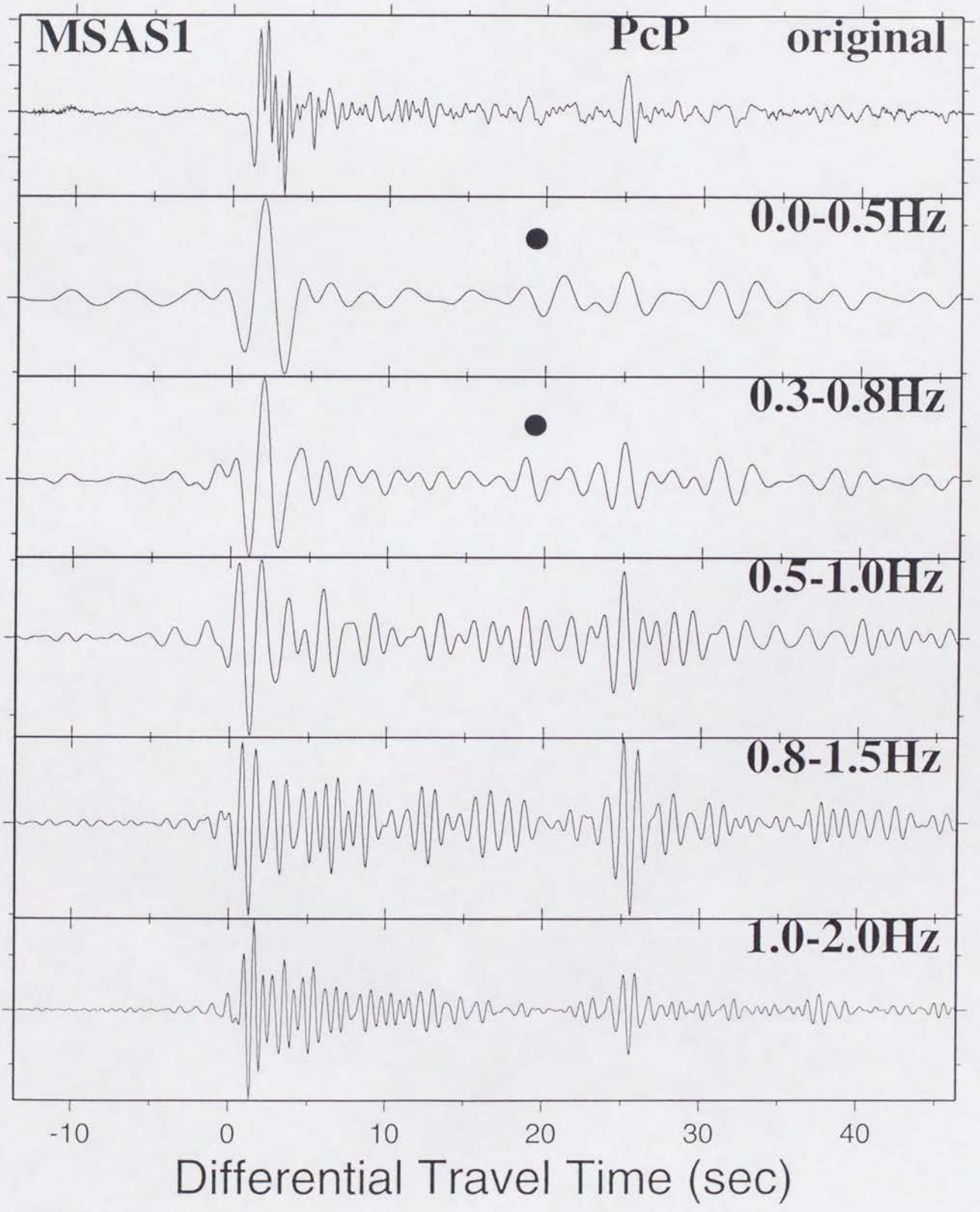
MSAS1
PcP
original
0.0-0.5Hz
0.3-0.8Hz
0.5-1.0Hz
0.8-1.5Hz
1.0-2.0Hz
-10
0
10
20
30
40
Differential Travel Time (sec)

Figure 6

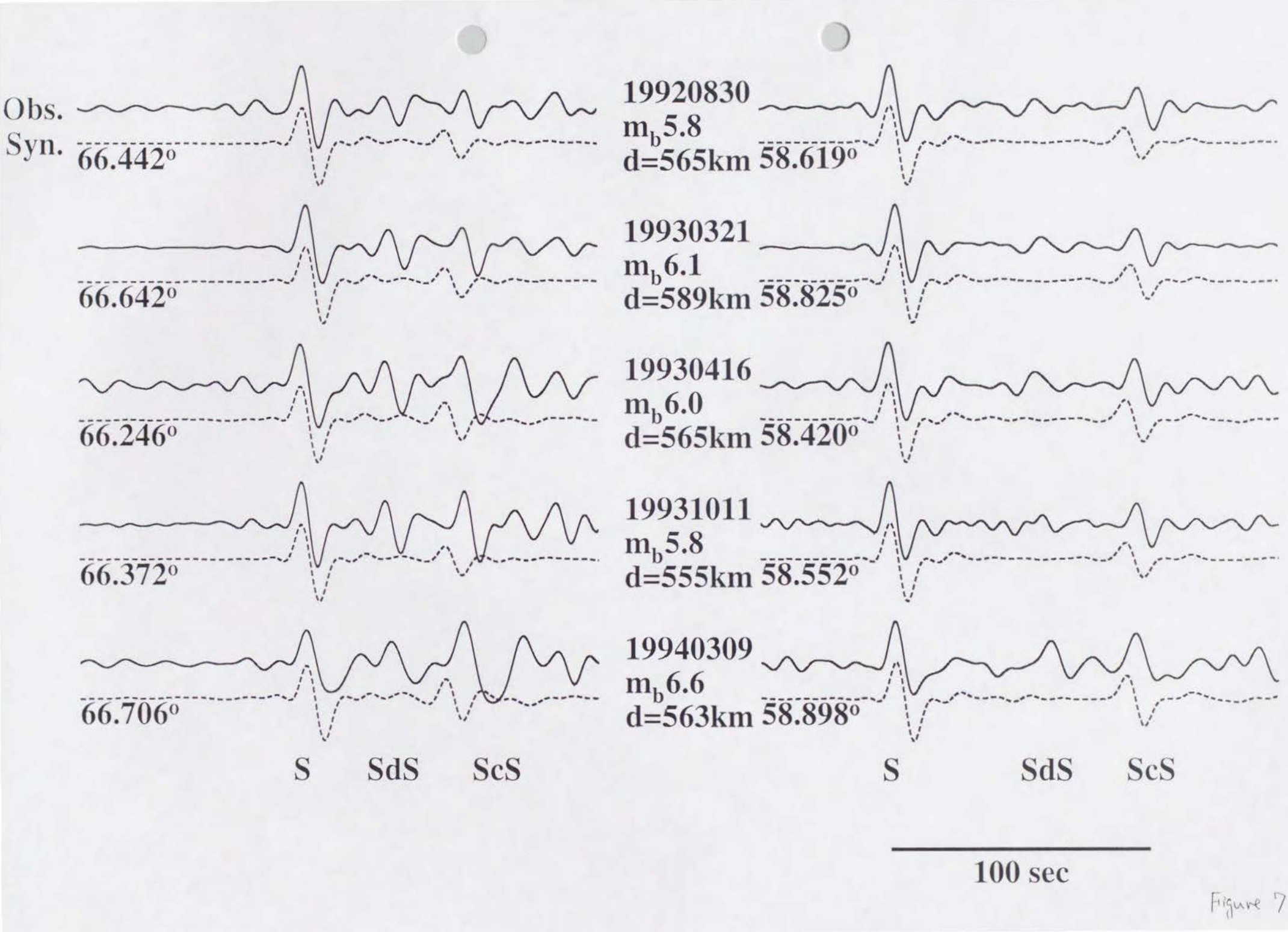
Obs.
Syn.
66.442°
19920830
m_b5.8
d=565km
58.619°
66.642°
19930321
m_b6.1
d=589km
58.825°
66.246°
19930416
m_b6.0
d=565km
58.420°
66.372°
19931011
m_b5.8
d=555km
58.552°
66.706°
19940309
m_b6.6
d=563km
58.898°
S
SdS
ScS
S
SdS
ScS
100 sec

Figure 7

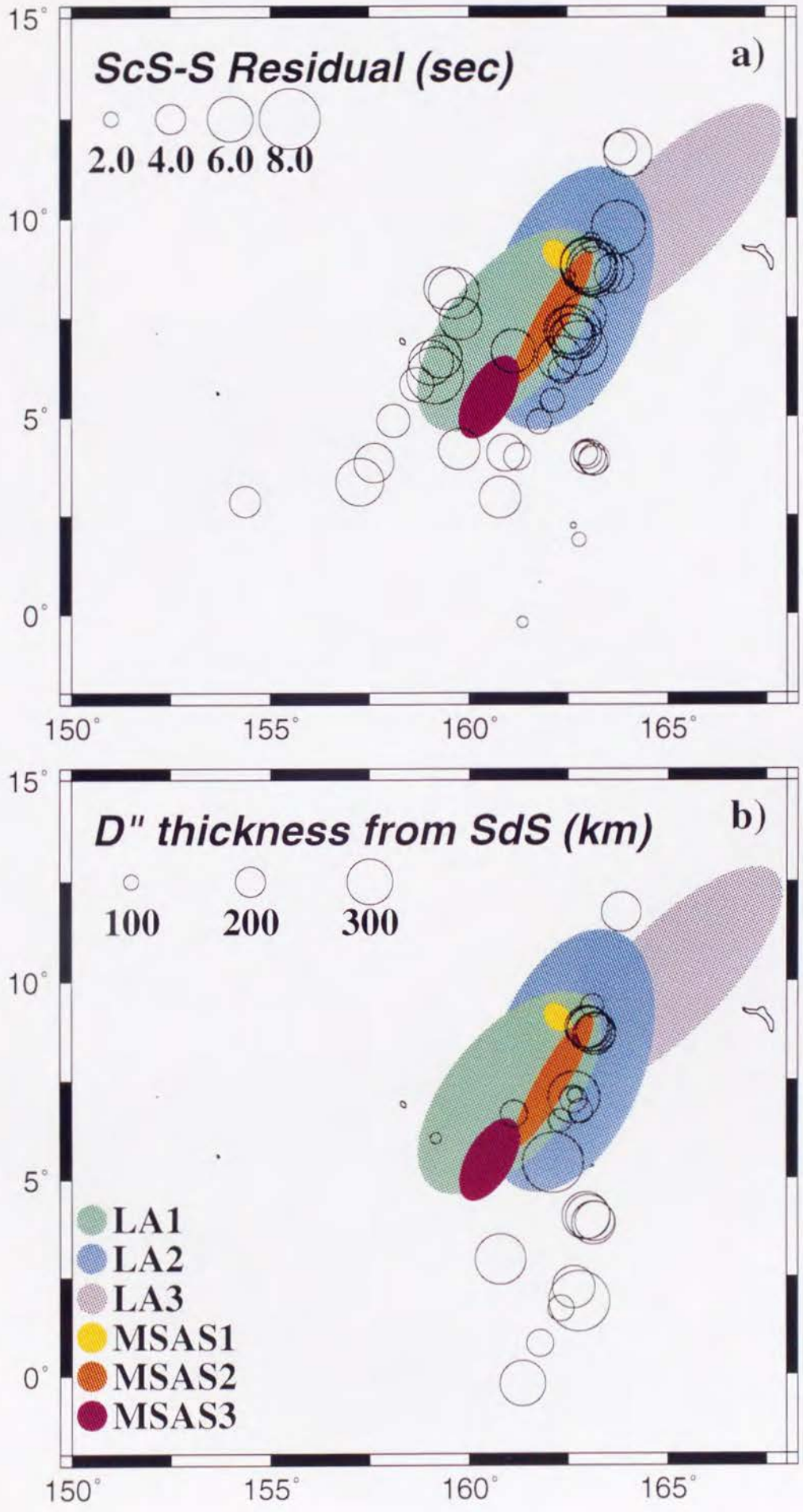
ScS-S Residual (sec)
a)
2.0 4.0 6.0 8.0
D" thickness from SdS (km)
b)
100 200 300
LA1
LA2
LA3
MSAS1
MSAS2
MSAS3
15°
10°
5°
0°
150°
155°
160°
165°

Figure 8

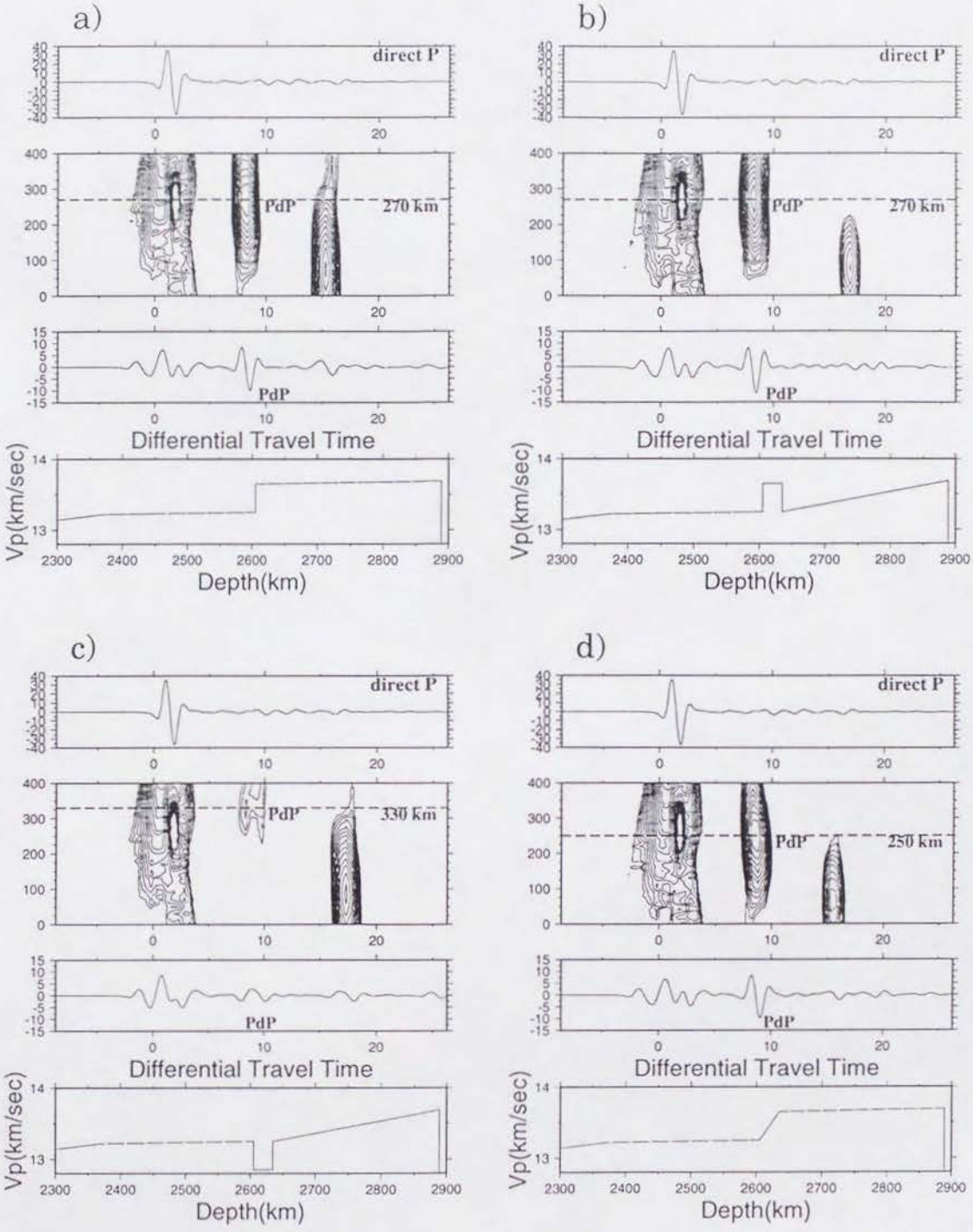
a)
direct P
PdP
270 km
PdP
Differential Travel Time
Vp(km/sec)
Depth(km)
b)
direct P
PdP
270 km
PdP
Differential Travel Time
Vp(km/sec)
Depth(km)
c)
direct P
PdP
330 km
PdP
Differential Travel Time
Vp(km/sec)
Depth(km)
d)
direct P
PdP
250 km
PdP
Differential Travel Time
Vp(km/sec)
Depth(km)

Figure 9

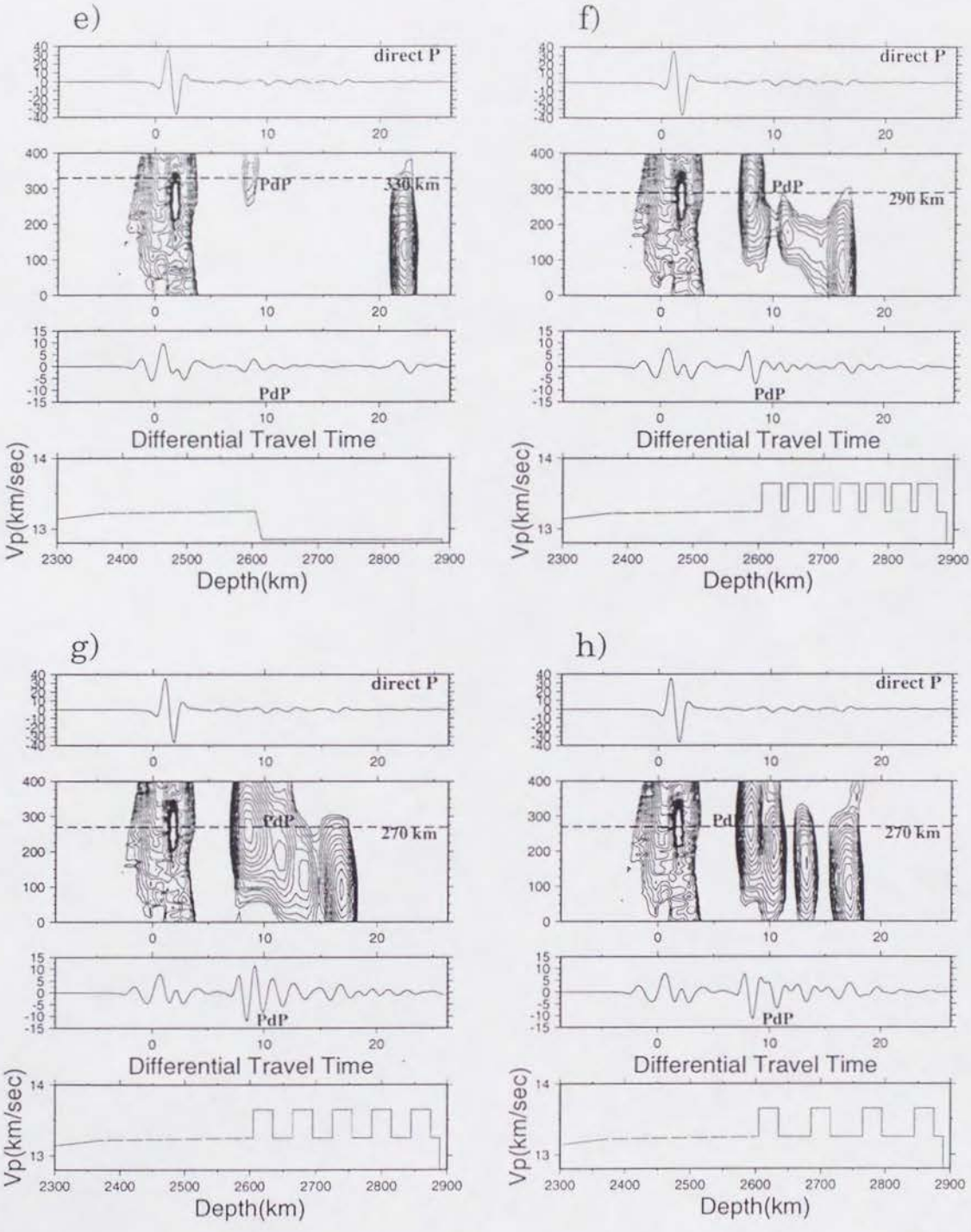

Figure 9 (Continued)

i)

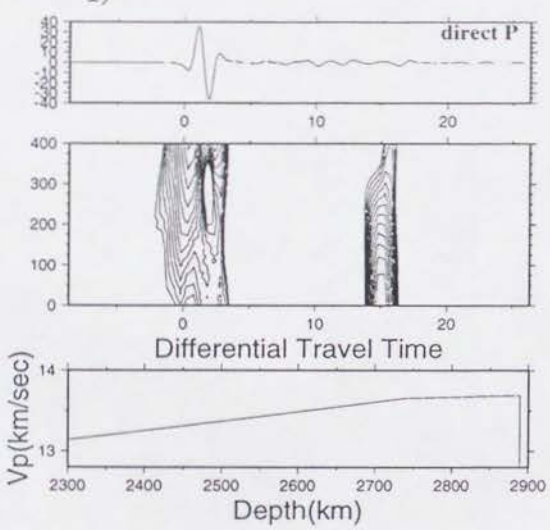

Figure 9 (Continued)

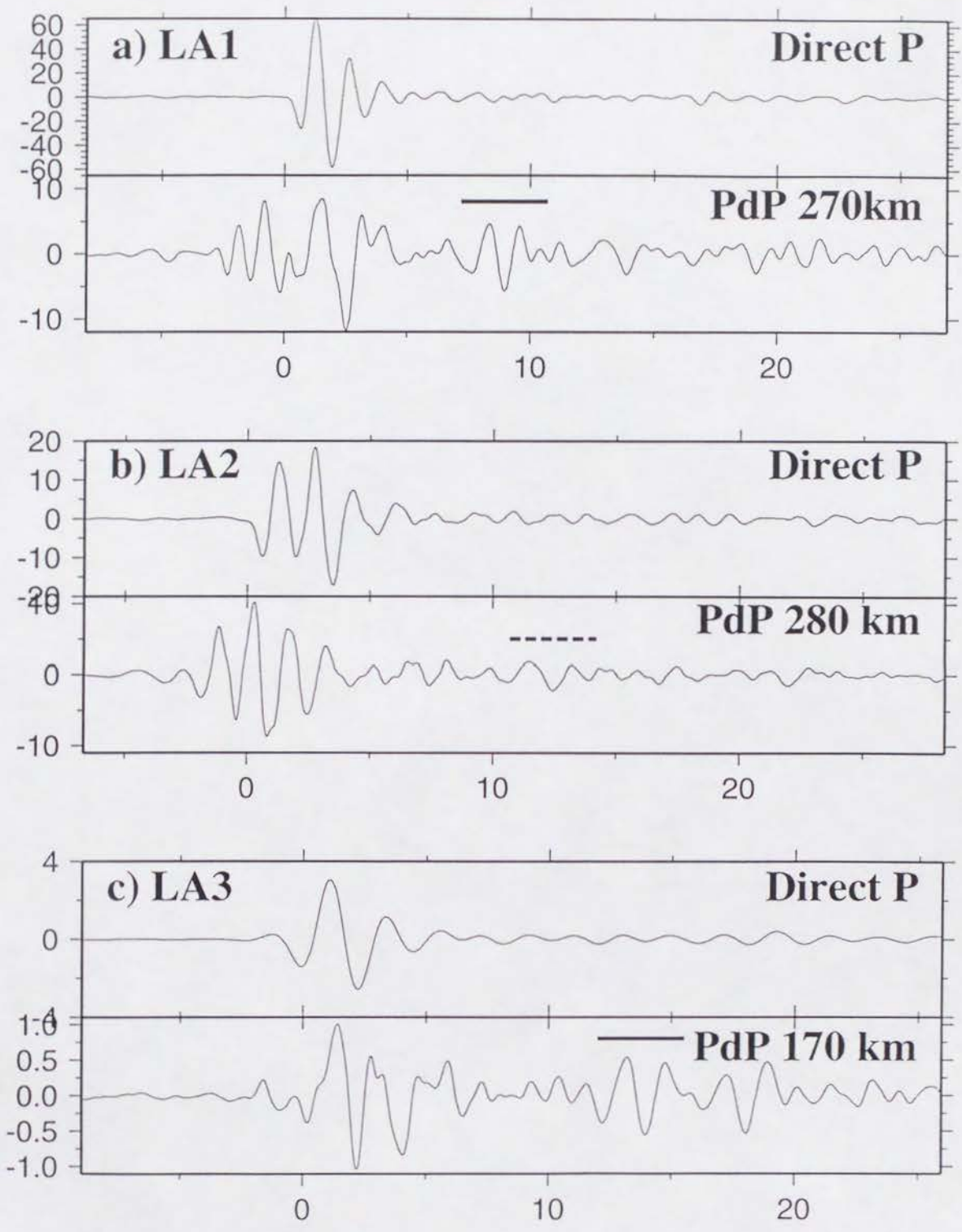
a) LA1
Direct P
PdP 270km
b) LA2
Direct P
PdP 280 km
c) LA3
Direct P
PdP 170 km

Figure 10

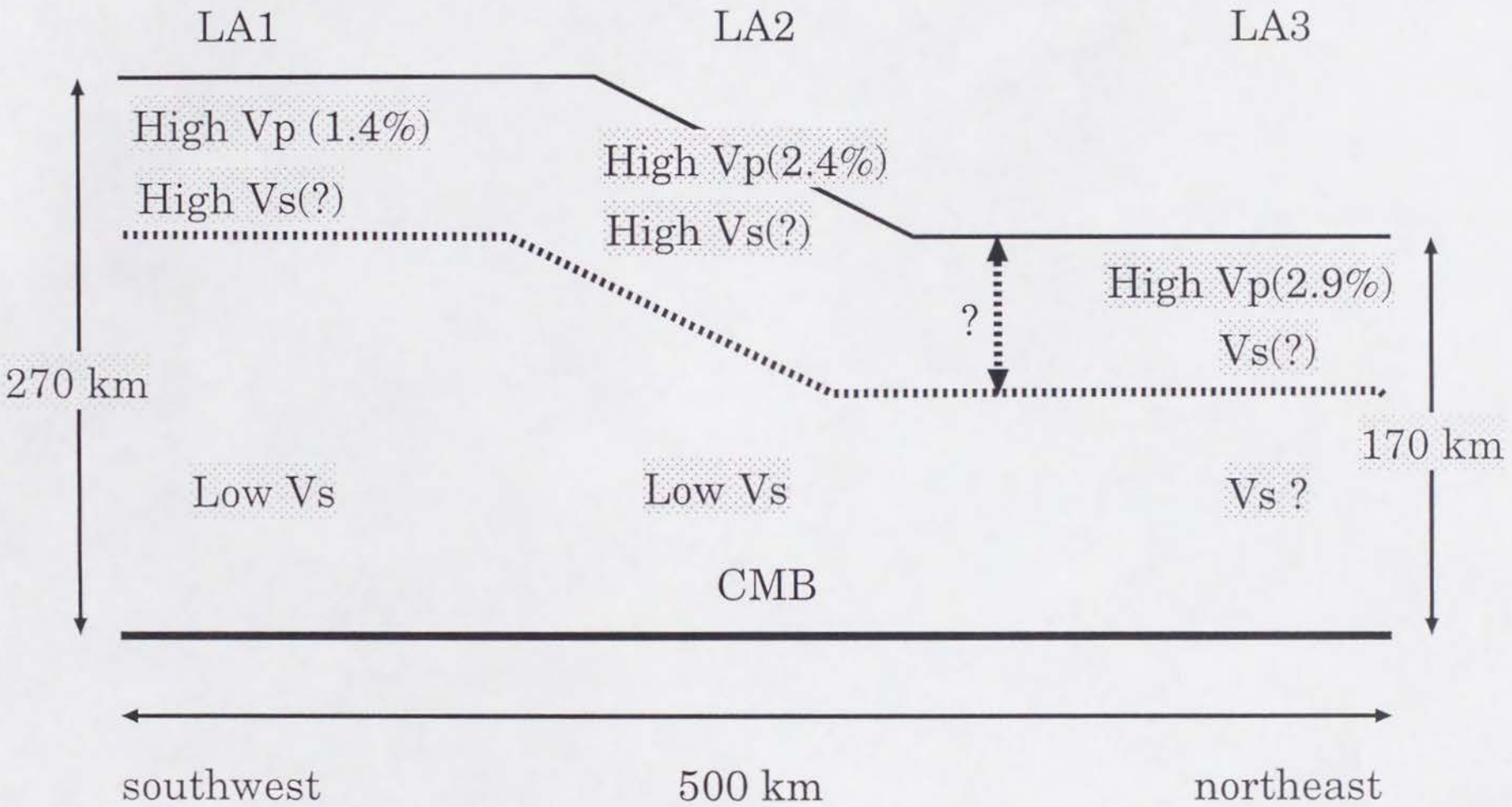
LA1
LA2
LA3
High Vp (1.4%)
High Vs(?)
High Vp(2.4%)
High Vs(?)
?
High Vp(2.9%)
Vs(?)
270 km
170 km
Low Vs
Low Vs
Vs ?
CMB
southwest
500 km
northeast

Figure 11

(e.g., the Indian Ocean), but is constant beneath mid ocean ridge (e.g., the Mid Atlantic Ridge).

Introduction

The mid ocean ridges (spreading regions) have been considered to play a passive role in the force balance of plate tectonics[5] and only shallow structure has been studied in detail[6]. Seismic tomography using surface waves[7,8] has a limited resolution in both horizontal and vertical direction, especially poor resolution in the depths and contrasts of the upper mantle discontinuities.

We examine the results of previous studies[1-4] by analysing the data from recent large deep earthquakes in Fiji and Bolivia, whose bounce points of P'P' are located near the Mid Atlantic Ridge and far from the Mid Indian Ocean Ridge, respectively. We show the regional difference of the underside reflections of P'P' from the 420- and the 660-km discontinuities (referred to as $P'_{420}P'$ and $P'_{660}P'$ here after) and attempt to interpret the differences in terms of chemical composition with an assumption of pyrolite mantle.

Data

The Fiji earthquake of March 9, 1994 (m_b= 6.6) and the Bolivian earthquake of June 9, 1994 (m_b= 7.0) provide us with a rare chance for the analysis of $P'_{420}P'$ and $P'_{660}P'$. We analyse the data of short-period vertical-component seismograms from the Fiji and Bolivian earthquakes recorded by the micro earthquake network

of Tohoku University and Southern California USGS-Caltech network. We use the hypocenter parameters listed in monthly PDE (Preliminary Determination of Epicenters) report to calculate the travel times and bounce points of P'P', P'$_{420}$P' and P'$_{660}$P'. Figure 1 shows that the bounce points for the Fiji earthquake are located close to the Mid Atlantic Ridge and that those for the Bolivian earthquake far from the Mid Indian Ocean Ridge. This difference of the bounce point locations encourages us to study structural difference of mantle beneath the mid ocean ridge and normal ocean. Strict inspection of all data by display of original traces and filtered traces obtained from several pass bands leads to 20 traces for the Fiji earthquake and 82 traces for the Bolivian earthquake. We use the short-period vertical-component seismograms filtered with a pass band of 0.2-0.5 Hz (Fig. 2). The epicentral distance ranges from 67.1 $^{\circ}$ to 70.2 $^{\circ}$ for the Fiji earthquake and 64.4 $^{\circ}$ to 70.5 $^{\circ}$ for the Bolivian earthquake.

Analysis

The slowness is one of important parameters to identify the underside reflections of P'P' from the upper mantle discontinuities. The slant-stacking of the filtered seismograms in Fig. 2 is made with a slowness interval of 0.1 sec/deg to measure the travel times and slownesses of significant signals in the data. The comparison of the calculated travel times and slownesses with those of clear peaks

in the contour maps indicates that P'$_{660}$P' from the Fiji earthquake (Fig. 3a), and P'$_{660}$P' and P'$_{420}$P' from the Bolivian earthquake (Fig. 3b) can be identified without ambiguity. The fact that the signals of P'$_{660}$P' and P'$_{420}$P' consist of three dominant peaks (Fig. 3b) is a strong evidence for the signals from the great Bolivian earthquake, because the waveforms of P waves recorded by broad-band instruments suggest that three dominant shocks occurred during the rupture process of the earthquake. Another apparent signal with slowness of -4.3 sec/deg (Fiji) and -4.3 sec/deg (Bolivia) is not interpreted as P'$_d$P' (d $<$ 420-km), but as SKKKP[9].

Figure 4a and 4b show the result of the slant-stacking with a slowness of -2.7 sec/deg for the Fiji and Bolivian earthquake, respectively. The signals of P'$_{660}$P' clearly show up for both earthquakes. The amplitude of P'$_{420}$P' is almost similar to that of P'$_{660}$P' for the Bolivian earthquake, but is buried in ambient noises in the case of the Fiji earthquake. These results in Figs. 3 and 4 are consistent with the previous array studies[1-4]. This is the first clear evidence for the regional variation of underside reflection of P'P' from the 420-km discontinuity since the pioneering studies[10-12] of precursors to P'P'. The seismological discovery of the present study is that there exists the difference of the reflectivity of the 420-km discontinuity between the area close (about 2 $^\circ$) to the Mid Atlantic Ridge and the area far away (about 20 $^\circ$) from the Mid Indian

Ocean Ridge. The data sets analysed in the present study does not show such a clear regional variation for the 660-km discontinuity. However, one of the array studies of $P'_dP'^2$ suggests the possibility of a weak reflectivity of the 660-km discontinuity beneath the Mid Atlantic Ridge.

Implications on chemical composition

Advances in high-pressure experiments have reached a depth of about 800 km in the Earth's mantle[13–15]. It may be possible for us to interpret the seismological results of the present study in terms of mineralogical phase relation. We assume Mg_2SiO_4-Fe_2SiO_4 system in the following discussion.

420-km discontinuity

Recent high pressure experiments[16,17] of olivine (α) to modified spinel (β) transformation, which is considered to correspond to the 420-km discontinuity, suggest the transformation width of 11 to 19 km in temperature range of 1400 to 1750 ℃ for the composition of $(Mg_{0.89}Fe_{0.11})SiO_4$[16], and the decrease of the width with temperature increase[16,18]. Our observational result from the Fiji earthquake is consistent with this experimental result. However, the clear reflection from the Bolivian earthquake seems inconsistent with the width range. An easy way to overcome this inconsistency is to change the Mg-Fe ratio from $(Mg_{0.89}Fe_{0.11})SiO_4$ beneath the discontinuity. They[16] infer that Mg content is greater than 95% or

smaller than 80%. We can suggest that the increase of Fe content to 17% beneath the discontinuity is plausible. The effect of H_2O[19] on the transformation should be investigated with careful experiment.

660-km discontinuity

Recent high pressure experiment[13] shows that the transformation of spinel to perovskite + magnesiowüstite take places at a pressure of 23 GPa with a pressure interval less than 0.15 GPa at a temperature of 1600 ℃. These pressure values are converted to a depth of 653 km and a depth interval less than 5 km. These values are consistent with the results of the present study for both the Fiji and Bolivian earthquakes.

One of the recent array studies[2] suggests the possibility of the reflectivity decrease with decreasing distance of the bounce points to the Mid Atlantic Ridge. This might require a change of chemical composition near the 660-km discontinuity across the Mid Atlantic Ridge.

Conclusion

An unambiguous regional variation of the reflectivity of 420-km discontinuity is observed between the bounce points close to the Mid Atlantic Ridge and those far away from the Mid Indian Ocean Ridge. The reflections from the 660-km discontinuity are clearly observed from the both bounce points. Recent array study[2] by one

of the authors of the present study finds an evidence for the change of reflectivity of the 660-km discontinuity beneath the Mid Atlantic Ridge.

Interpretation of these results in terms of chemical composition is not unique. However, the change of chemistry near the discontinuities is a simple but most plausible interpretation. Interpretation by temperature variation seems difficult. The focussing and defocussing due to heterogeneities in the Earth cannot be ruled out. We must point out that the bounce points for the Fiji earthquake are close to a hot spot[20] (Fig. 1(a)). There found no hot spot near the bounce points for the Bolivian earthquake.

Acknowledgments.

The data analysed in this study were provided by courtesy of Tohoku University and California Institute of Technology.

References

1. Nakanishi, I., Seismic reflections from the upper mantle discontinuities beneath the Mid-Atlantic Ridge observed by a seismic array in Hokkaido region, Japan, Geophys. Res. Lett., 13, 1458-1461, 1986

2. Nakanishi, I., Reflections of P'P' from upper mantle discontinuities beneath the Mid-Atlantic Ridge, Geophys. J. R. Astron. Soc., 93, 335-346, 1988

3. Nakanishi, I., A search for topography of the mantle discontinuities from precursors to P'P', J. Phys. Earth, 37, 297-301, 1989

4. Benz, H. M. and J. E. Vidale, Sharpness of upper-mantle discontinuities determined from high-frequency reflections, Nature, 365, 147-150, 1993

5. Forsyth, D. and S. Uyeda, On the relative importance of the driving forces of plate motion, Geophys. J. R. Astron. Soc., 43, 163-200, 1975

6. Detrick, R. S., P. Buhl, E. Vera, J. Mutter, J. Orcutt, J. Madsen, and T. Brocher, Multi-channel seismic imaging of a crustal magma chamber along the East Pacific Rise, Nature, 326, 35-41, 1987

7. Nakanishi, I. and D. L. Anderson, Measurements of mantle wave velocities and inversion for lateral heterogeneity and anisotropy-II. Analysis by the single-station method, Geophys. J. R. Astron. Soc., 78, 573-617, 1984

8. Woodhouse, J. H. and A. M. Dziewonski, Mapping the upper mantle: Three-dimensional modeling of Earth structure by inversion of seismic waveforms, J. Geophys. Res., 89, 5953-5986, 1984

9. Engdahl, E. R. and E. A. Flinn, Remarks on the paper "Early reflections of P'P' as an indication of upper mantle structure," by R. D. Adams, Bull. Seism. Soc. Am., 59, 1415-1417, 1969

10. Engdahl, E. R. and E. A. Flinn, Seismic waves reflected from discontinuities within Earth's upper mantle, Science, 163, 177-179, 1969

11. Whitcomb, J. H. and D. L. Anderson, Reflection of P'P' seismic waves from discontinuities in the mantle, J. Geophys. Res., 75, 5713-5728, 1970

12. Adams, R. D., Reflections from discontinuities beneath Antarctica, Bull. Seism. Soc. Am., 61, 1441-1451, 1971

13. Ito, E. and E. Takahashi, Postspinel transformations in the system Mg_2SiO_4-Fe_2SiO_4 and some geophysical implications, J. Geophys. Res., 94, 10637-10646, 1989

14. Anderson, D. L., Theory of the Earth, Blackwell Scientific Publications, Boston, 1989

15. Irifune, T., Phase transformations in the earth's mantle and subducting slabs: Implications for their compositions, seismic velocity and density structures and dynamics, The Island Arc, 2, 55-71, 1993

16. Katsura, T. and E. Ito, The system Mg_2SiO_4-Fe_2SiO_4 at high pressures and temperatures: Precise determination of stabilities of olivine, modified spinel, and spinel, J. Geophys. Res., 94, 15663-15670, 1989

17. Akaogi, M., E. Ito, and A. Navrotsky, Olivine-modified spinel-spinel transitions in the system Mg_2SiO_4-Fe_2SiO_4: Calorimetric measurements, thermochemical calculation, and geophysical application, J. Geophys. Res., 94, 15671-15685, 1989

18. Helffrich, G. and C. R. Bina, Frequency dependence of the visibility and depths of mantle seismic discontinuities, Geophys. Res. Lett., 21, 2613-2616, 1994

19. Wood, B. J., The effect of H_2O (water) on the 410-kilometer seismic discontinuity, Science, 268, 74-76, 1995

20. Turcotte, D. L. and G. Schubert, Geodynamics: Applications of continuum physics to geological problems, John Wiley & Sons, 450pp, 1982

Figure Captions

Figure 1. Surface bounce points (solid circle) of P'P'. The locations of hot spots[20] (solid stars) are also shown. (a)Fiji-Japan. (b)Bolivia-Southern Carifornia.

Figure 2. Short-period vertical-component seismograms filtered with a pass band of 0.2-0.5Hz. (a)Fiji-Japan. (b)Bolivia-Southern Carifornia.

Figure 3. Contour map showing the result of slant-stacking of the filtered seismograms in Fig. 2. Also shown are the locations of P'P', $P'_{420}P'$, $P'_{660}P'$, and SKKKP. (a)Fiji-Japan. (b)Bolivia-Southern Carifornia.

Figure 4. Cross-section of Fig. 3 for a constant slowness of -2.7 sec/deg. Also shown are the locations of P'P', $P'_{420}P'$, $P'_{660}P'$. (a)Fiji-Japan. (b)Bolivia-Southern Carifornia.

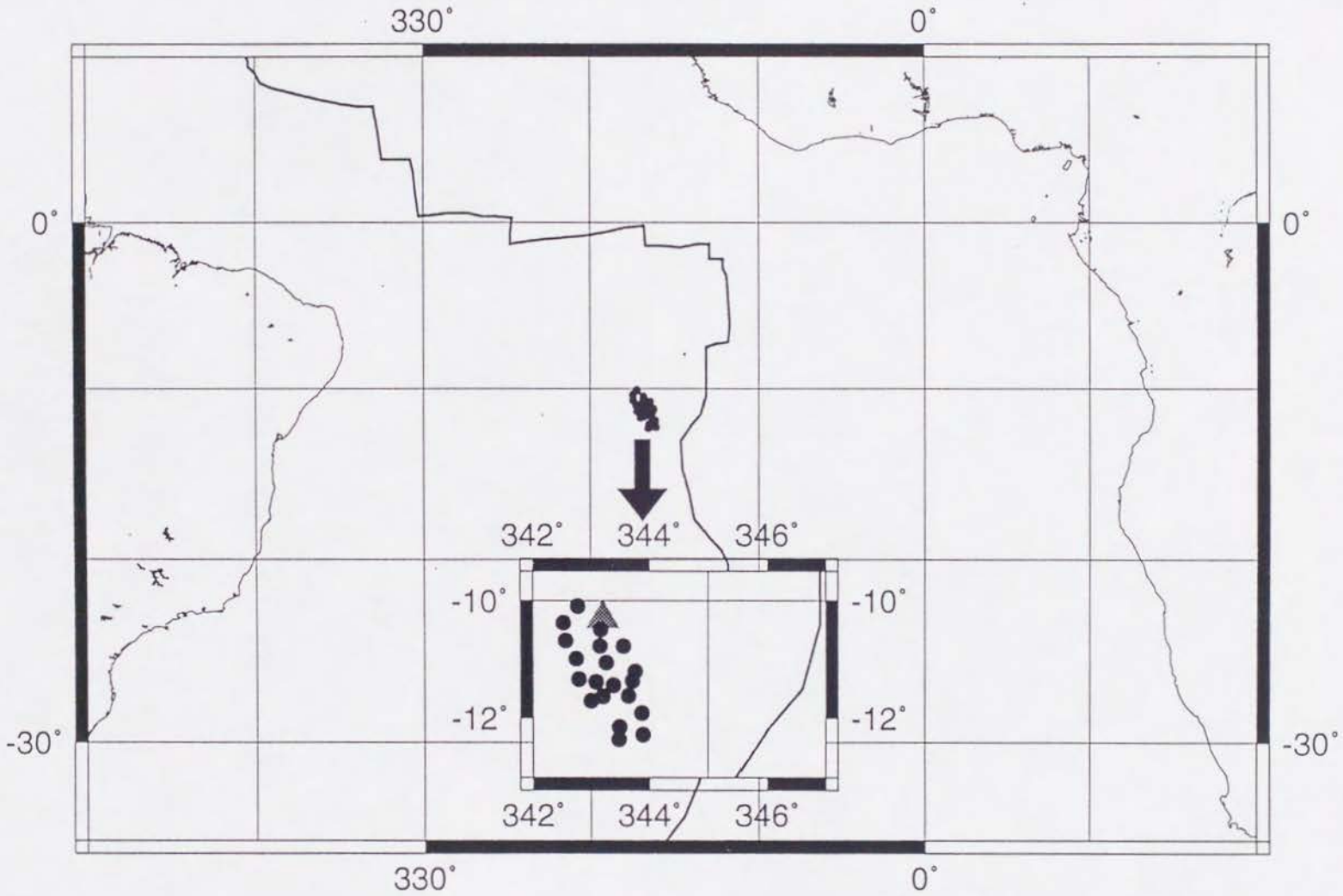

Fig. 1 (a)

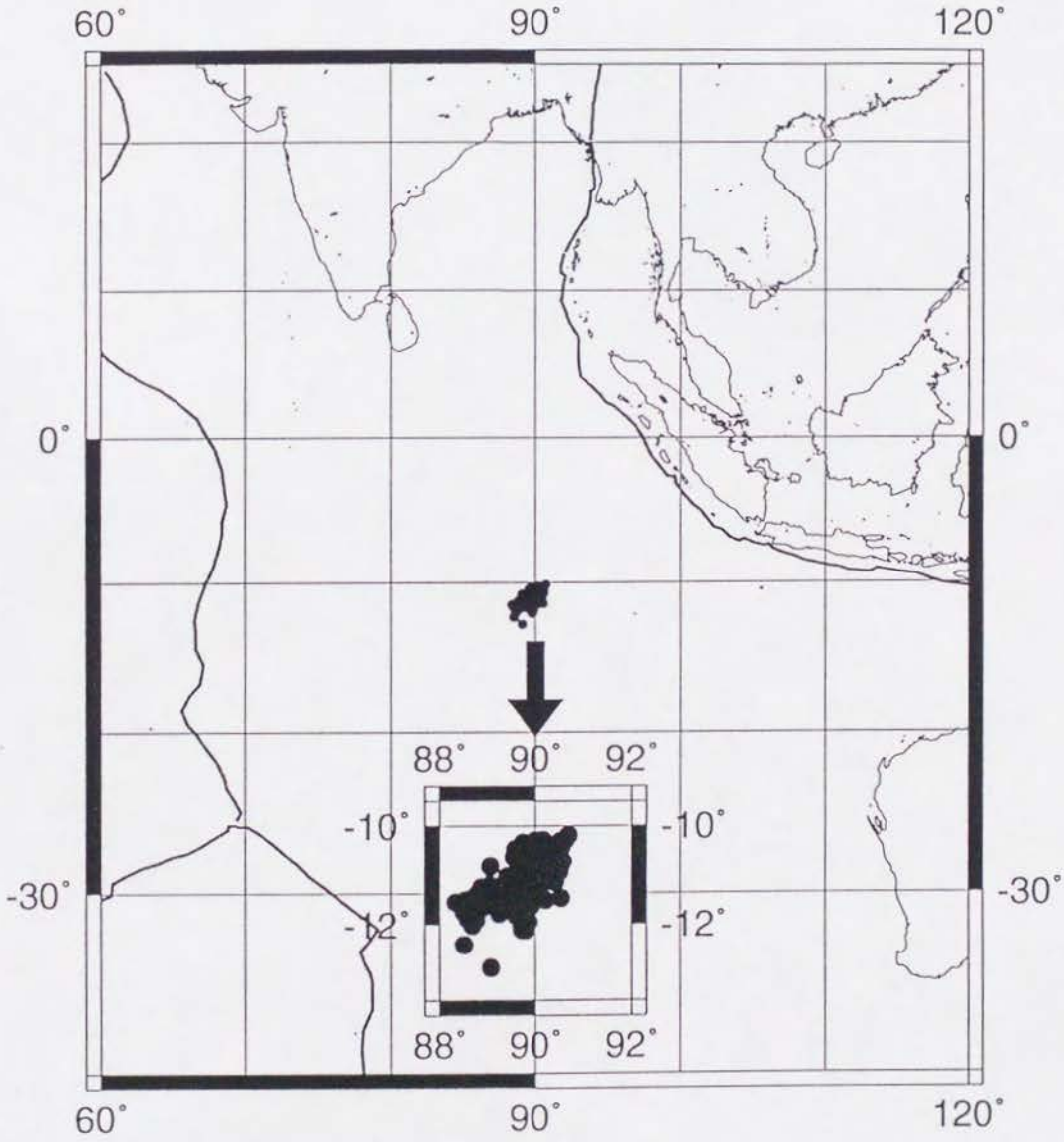

Fig. 1 (b)

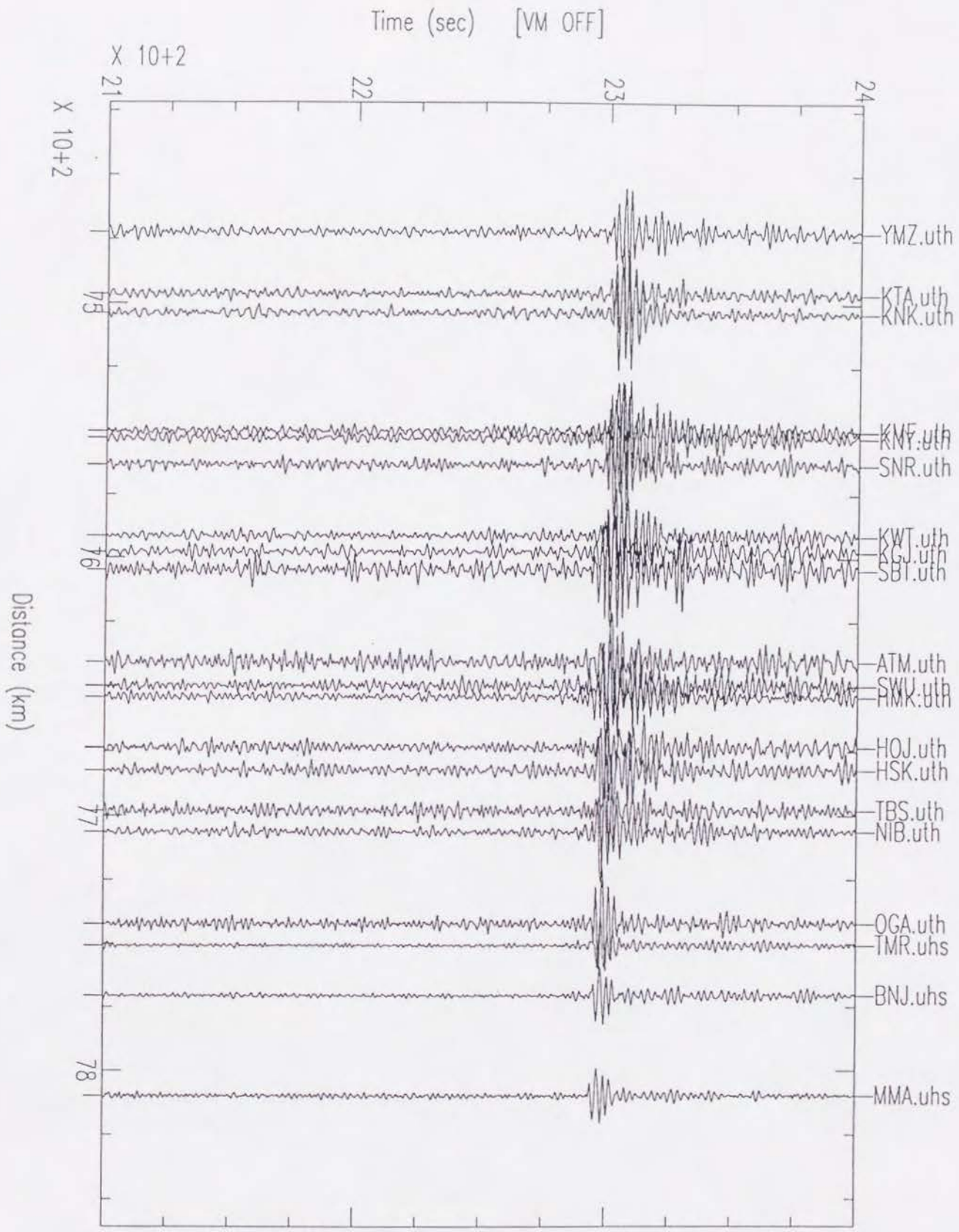
Time (sec) [VM OFF]
X 10+2
21
22
23
24
X 10+2
75
76
77
78
Distance (km)
YMZ.uth
KTA.uth
KNK.uth
KMF.uth
SNR.uth
KWT.uth
KGJ.uth
SBT.uth
ATM.uth
SWU.uth
HMK.uth
HOJ.uth
HSK.uth
TBS.uth
NIB.uth
OGA.uth
TMR.uhs
BNJ.uhs
MMA.uhs

Fig. 2(a)

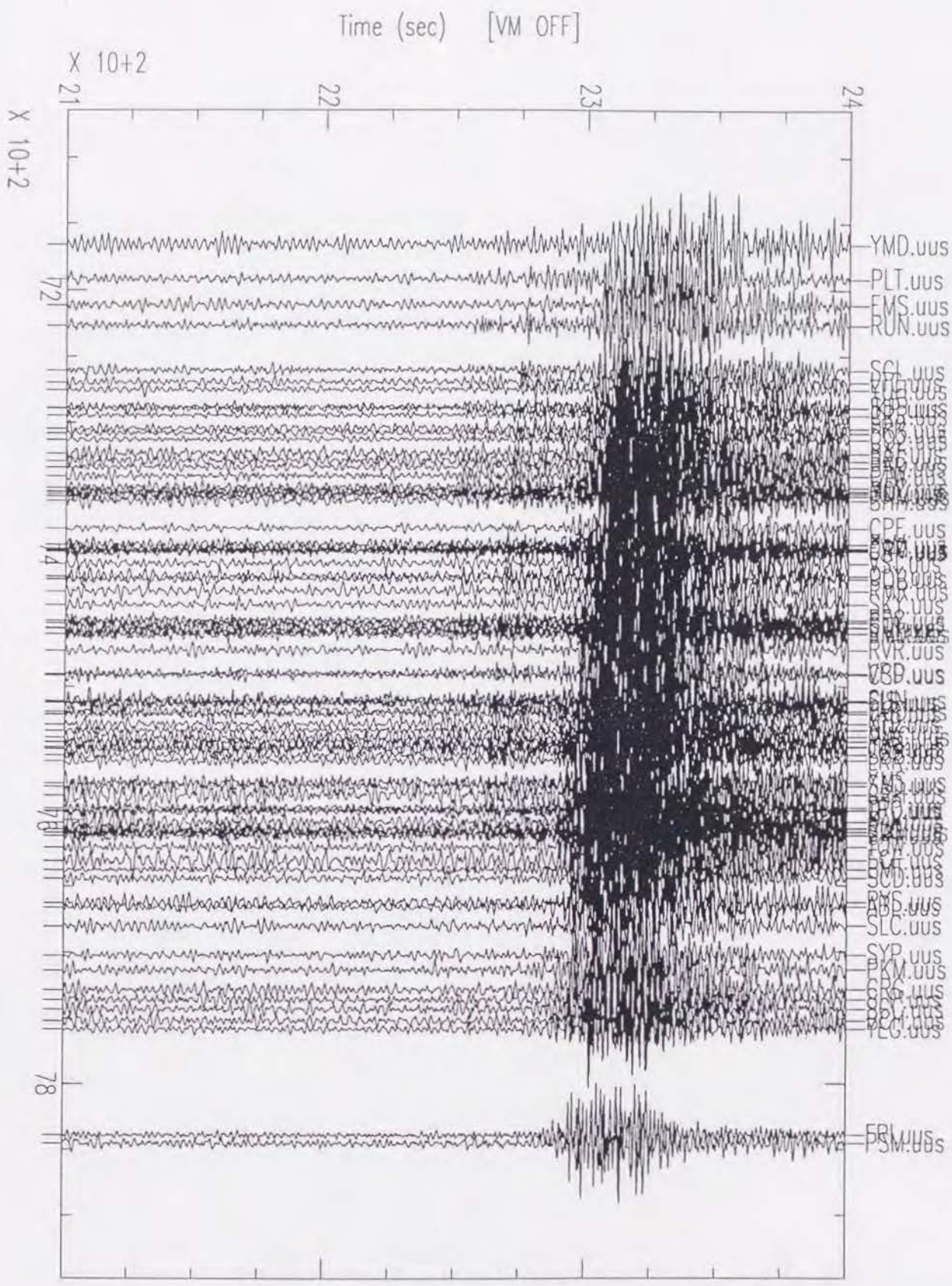
Time (sec) [VM OFF]
X 10+2
21
22
23
24
X 10+2
72
74
76
78
Distance (km)
YMD.uus
PLT.uus
EMS.uus
RUN.uus
SCL.uus
CPE.uus
RVR.uus
CBD.uus
SCD.uus
ABD.uus
SLC.uus
SYP.uus
PKM.uus
PEG.uus
PSM.uus

Fig. 2(b)

Fig. 3 (a)

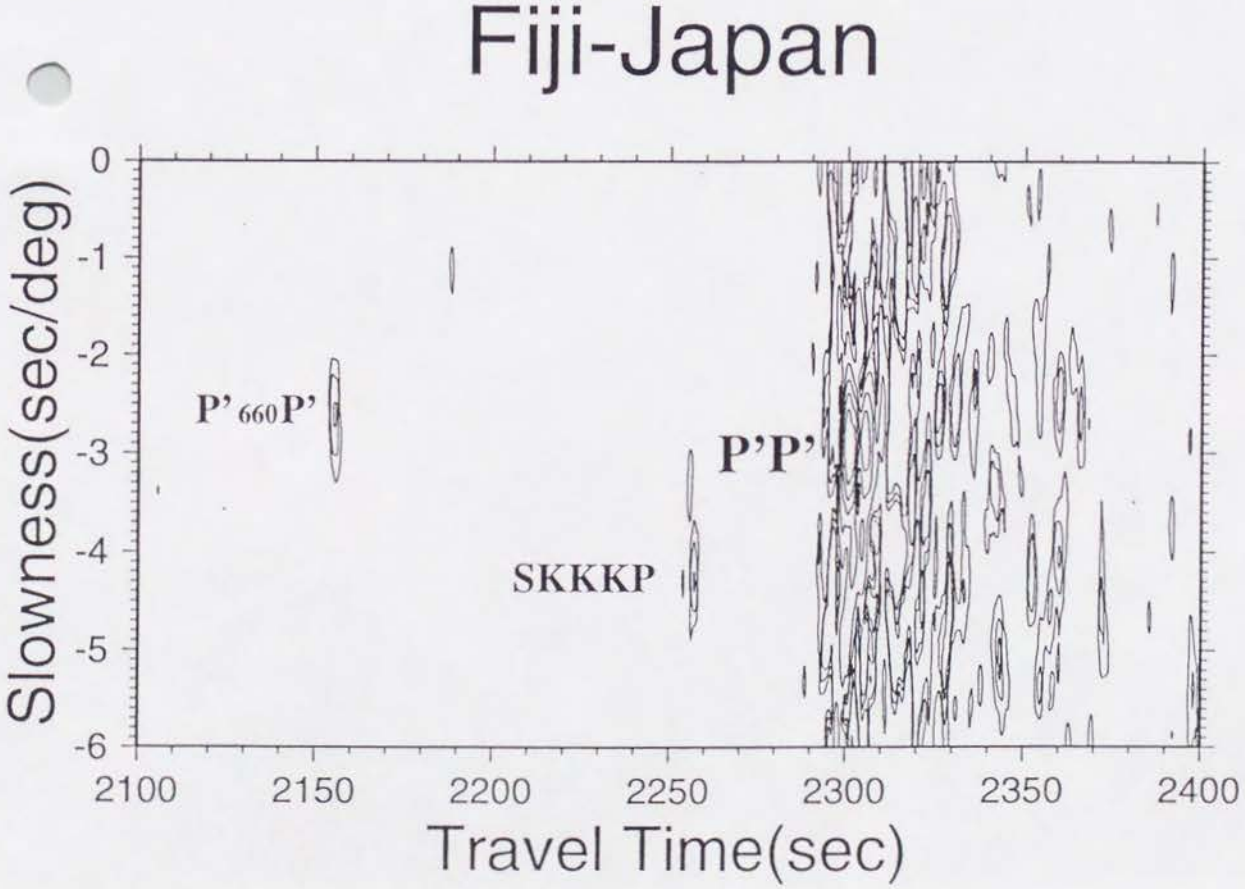
Fiji-Japan
Slowness(sec/deg)
0
-1
-2
-3
-4
-5
-6
P'660P'
P'P'
SKKKP
2100
2150
2200
2250
2300
2350
2400
Travel Time(sec)

Fig. 3(b)

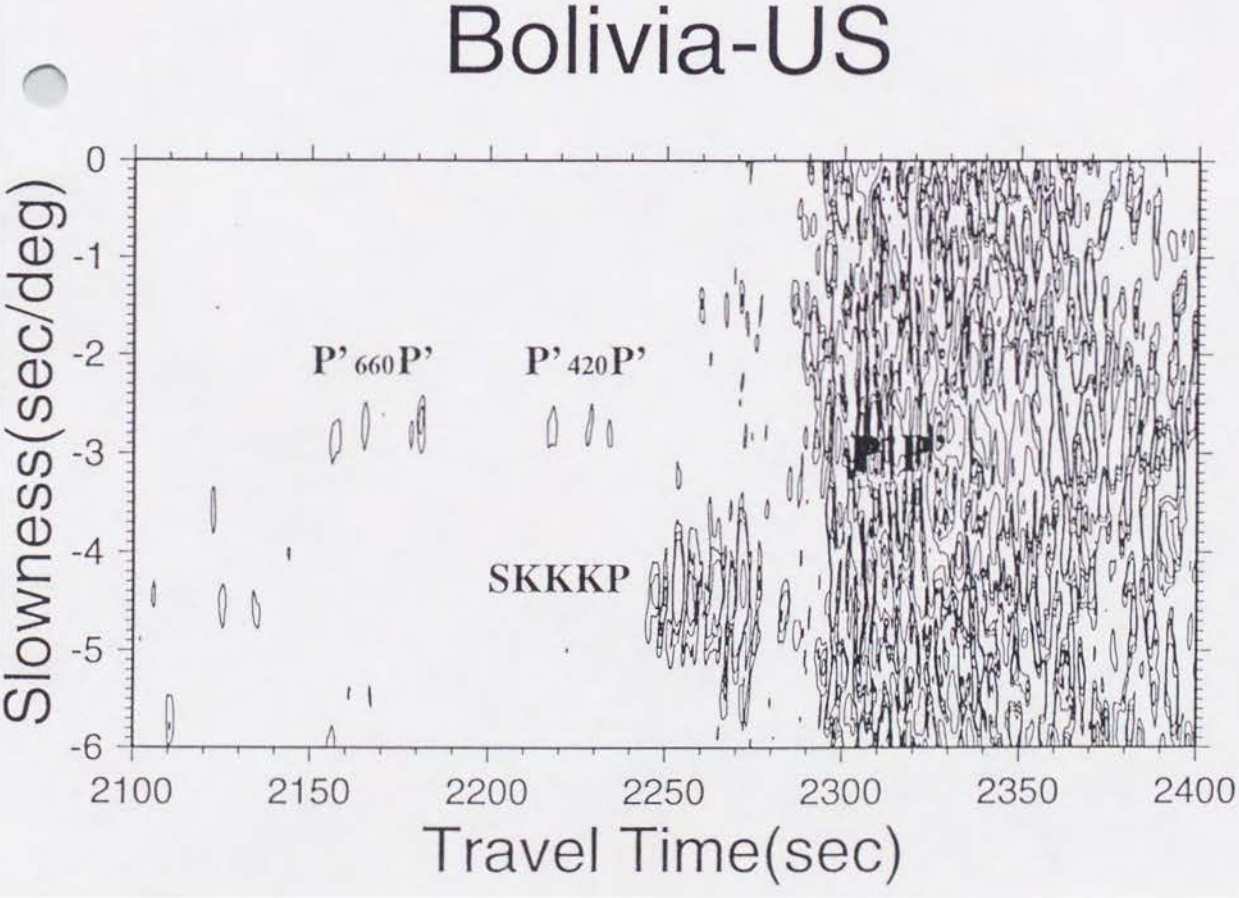
Bolivia-US
Slowness(sec/deg)
0
-1
-2
-3
-4
-5
-6
P'660P'
P'420P'
PP'
SKKKP
2100
2150
2200
2250
2300
2350
2400
Travel Time(sec)

Fiji-Japan

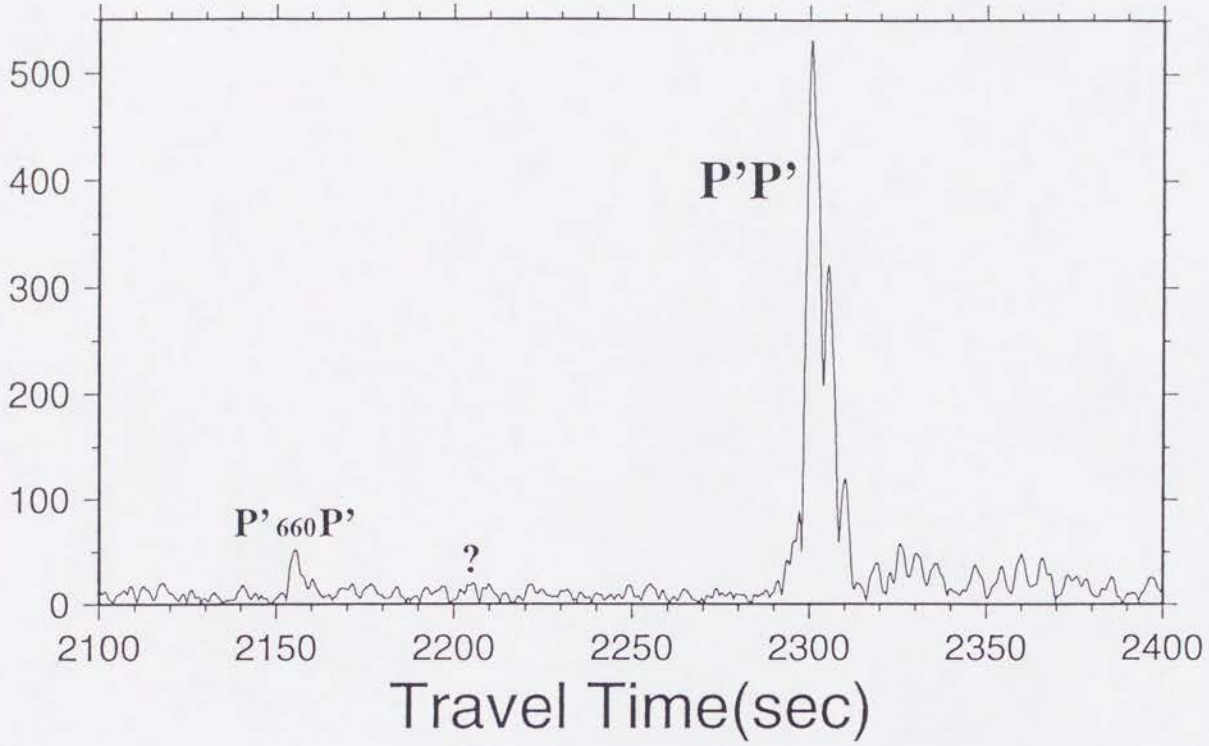

Fig. 4(a)

Bolivia-US

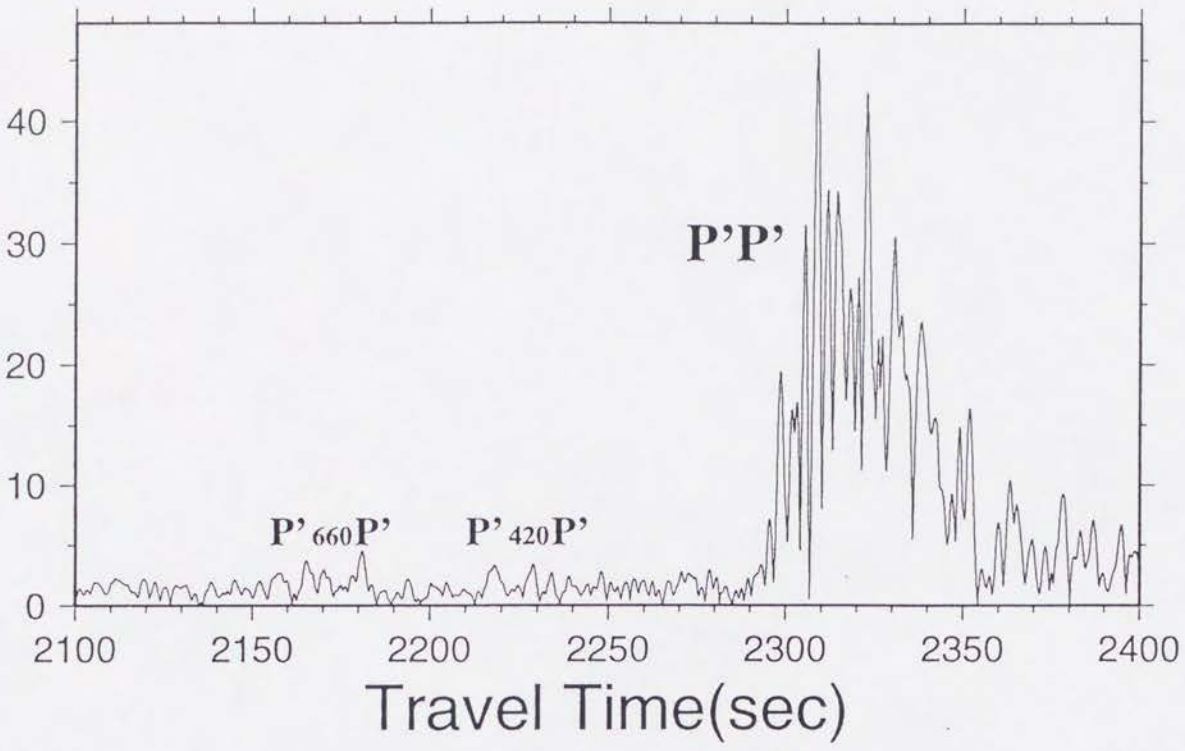

Fig. 4 (b)